ROYAL INSTITUTE
OF TECHNOLOGY

Feedback and Adjoint Based Control of Boundary Layer Flows

by

Mattias Chevalier

December 2004
Technical Reports from
Royal Institute of Technology
Department of Mechanics
SE-100 44 Stockholm, Sweden

Typsatt i $\mathcal{AMS}$-LaTeX.

Akademisk avhandling som med tillstånd av Kungliga Tekniska Högskolan i Stockholm framlägges till offentlig granskning för avläggande av teknologie doktorsexamen tisdagen den 7:e december 2004 kl. 10.15 i Kollegiesalen, Administrationsbyggnaden, Kungliga Tekniska Högskolan, Valhallavägen 79, Stockholm.

Edita Norstedts Tryckeri, Stockholm 2004

Till Anna och Ida

Feedback and Adjoint Based Control of Boundary Layer Flows

Mattias Chevalier
Department of Mechanics, Royal Institute of Technology
S-100 44 Stockholm, Sweden

Abstract

Linear and nonlinear optimal control have been investigated in transitional channel and boundary layer flows. The flow phenomena that we study are governed by the incompressible Navier–Stokes equations and the main aim with the control is to prevent transition from laminar to turbulent flows. A linear model-based feedback control approach, that minimizes an objective function which measures the perturbation energy, can be formulated where the Orr–Sommerfeld/Squire equations model the flow dynamics. A limitation with the formulation is that it requires complete state information. However, the control problem can be combined with a state estimator to relax this requirement. The estimator requires only wall measurements to reconstruct the flow in an optimal manner.

Physically relevant stochastic models are suggested for the estimation problem which turns out to be crucial for fast convergence. Based on these models the estimator is shown to work for both infinitesimal as well as finite amplitude perturbations in direct numerical simulations of a channel flow at $Re_{cl} = 3000$.

A stochastic model for external disturbances is also constructed based on statistical data from a turbulent channel flow at $Re_\tau = 100$. The model is successfully applied to estimate a turbulent channel flow at the same Reynolds number.

The combined control and estimation problem, also known as a compensator, is applied to spatially developing boundary layers. The compensator is shown to successfully reduce the perturbation energy for Tollmien–Schlichting waves and optimal perturbations in the Blasius boundary layer. In a Falkner–Skan–Cooke boundary layer the perturbation energy of traveling and stationary cross-flow disturbances are also reduced.

A nonlinear control approach using the Navier–Stokes equations and the associated adjoint equations are derived and implemented in the context of direct numerical simulations of spatially-developing three-dimensional boundary layer flows and the gradient computation is verified with finite-differences. The nonlinear optimal control is shown to be more efficient in reducing the disturbance energy than feedback control when nonlinear interactions are becoming significant in the boundary layer. For weaker disturbances the two methods are almost indistinguishable.

Descriptors: transition control, flow control, feedback control, optimal control, objective function, Orr–Sommerfeld/Squire equations, boundary layer flow, Falkner–Skan–Cooke flow, Navier–Stokes equations, Riccati equation, adjoint equations, DNS, estimation, LQG.

Preface

This thesis considers the study of feedback and adjoint based control in different boundary layer flows. The thesis is divided in two parts where the first part is an introduction to the research topic and an overview and summary of the present contribution to the field of fluid mechanics. The second part consists of five papers. A guide to the papers and the contributions of different authors is included in the last chapter of part one.

The five papers in part two are adjusted to comply with the present thesis format for consistency, but their content have not been altered compared to published versions except for minor refinements and corrections.

Stockholm, November 2004
Mattias Chevalier

Contents

Part 1

Overview and summary

CHAPTER 1

Overview

1.1. Introduction

The interest in controlling complex physical phenomena has grown as the need for and the possible benefits from this knowledge have become clearer, both economically but also environmentally. The field of aerodynamics is no exception. For example, large amounts of money could be saved if one could lower the fuel consumption of an airplane by just a fraction. Controlling the flow around the aircraft might be one way to achieve that.

A fluid motion over any surface includes a thin region, called a *boundary layer*, in which the flow is accelerated from rest to the freestream velocity a short distance above the surface. If disturbances are introduced in the boundary layer, for example through wall roughness, acoustic waves, or freestream turbulence, these disturbances can lead to transition from *laminar* to *turbulent* flows. A flow is laminar when the fluid motion is smooth and regular. The turbulent state on the other hand is characterized by rapidly varying velocities in both time and space. The transition phase that occurs between the laminar and turbulent flow has been and still is an area of intensive research. Through a better physical understanding of transition to turbulence it is also easier to understand how to control the different phases.

In many aerodynamic applications it is preferable to have a laminar flow since the friction drag gets lower. For example by extending the laminar flow regions on wings the drag can be reduced and the fuel consumption would decrease as a consequence. In other applications a turbulent flow state is preferable, for example in combustion engines where optimal mixing is desirable.

The transition phase is especially interesting, in terms of control, because we have the prospect of preventing or delaying transition to turbulence by controlling strong inherent instabilities using only minute control efforts.

Flow control, as a concept, covers all kinds of efforts to control flow phenomena. Interest in different aspects of flow control goes back hundreds of years and this interest has now grown into a well-established research area. The notion of flow control includes a wide variety of both methods and applications and a classification of those methods is useful. The first distinction is whether energy is fed into the flow or not. In *passive* control methods the flow field is altered without any energy addition. One classical example is the golf ball that would fly shorter if it had no dimples. The dimples trigger turbulence

which in turn delay separation and drag is reduced. In *active* control methods, an energy input to the flow is required. This can be done in two ways, either in a predetermined manner, open loop, or in a closed loop form, where some measurements are input to the control loop. The latter method is also known as *feedback control*, which emanates from the fact that measurements of the state is fed back to the controller that *reacts* on the basis of that information.

To construct effective control algorithms a thorough understanding of the underlying physics is needed. However since flow phenomena can be complex and non-intuitive the optimal control can be difficult to find solely based on intuition and knowledge. Therefore we would like to construct the control algorithm in such a way that as little as possible a priori knowledge about the flow is needed. This can be achieved by incorporating modern control theories that more systematically approach the design of the controller. This has been done during the last decade, however, to be able to apply these more advanced feedback flow control algorithms, appropriate sensors and actuators that can sense and act on sufficiently small scales in the flow, are needed. A rapid development in Micro-electro-mechanical systems (MEMS) technology has lead to laboratory experiments with promising devices.

In this thesis different methods of optimal control have been investigated by means of numerical experiments. The main aim has been to prevent transition to turbulence in boundary layer flows by applying blowing and suction control on the boundary. The final goal is to be able to apply the control algorithms to engineering applications but more work has to be done before active optimal control algorithms have reached that state.

Due to the fact that we study flow control through numerical simulations we are limited to low Reynolds numbers and simple geometries. On the other hand, as opposed to an experiment, we can get complete information about the flow state at all times which makes it easier to evaluate and understand different control strategies.

1.2. Optimal control

During the last decade, new approaches to solve flow control problems have emerged. By formulating the flow control problems as optimization problems where one wants to minimize or maximize some flow properties, one obtains a problem similar to what is studied in *optimal control* theory. The early publications regarding optimal flow control problems, such as Abergel & Temam (1990), Glowinski (1991), Gunzburger *et al.* (1989), Sritharan (1991*a*), Sritharan (1991*b*), and Gunzburger *et al.* (1992) are mostly concerned with theoretical aspects of the optimal control problem. Once the theoretical foundation was built, subsequent publications present results from numerical simulations where the optimal control for different flow configurations was computed.

When formulating an optimal control problem we need to have a model that describes the dynamics of the flow. We also need an objective function

that determines what we want to target with the control. Finally we also need to decide the means of control.

A major distinction is whether the governing equations are linear or nonlinear. The nonlinear optimization problems are computationally expensive to solve and the control works only for the very conditions it is designed for. This condition can be relaxed however through a robust control formulation, see e.g. Bewley *et al.* (2000). Examples of nonlinear control are given Joslin *et al.* (1997) where the optimal control of spatially growing two-dimensional disturbances in a boundary layer over a flat plate is computed. In Berggren (1998) the vorticity is minimized in an internal unsteady flow using blowing and suction on a part of the boundary and in Bewley *et al.* (2001) a turbulent flow at $Re_\tau = 180$ is completely relaminarized also using blowing and suction control which was shown in a direct numerical simulations. Other examples of successful application of nonlinear optimal control are given in Collis *et al.* (2000) where the flow dynamics is modeled in large eddy simulations and in He *et al.* (2000) where two different control approaches are successfully tested to reduce the drag resulting from the flow around a cylinder. The first approach is to use cylinder rotations to control the flow and the other is to use blowing and suction on parts of the cylinder wall.

The first linear feedback control schemes based on modern control theory are reported in Hu & Bau (1994) and Joshi *et al.* (1995). In these works closed loop control is achieved by stabilizing unstable eigenvalues. In Joshi *et al.* (1995) also model reduction is applied. In Bewley & Liu (1998) the control and estimation problem were studied separately for single wavenumber pairs. Transfer functions were used to evaluate the performance. The linear controller was then applied to larger problems. In Högberg *et al.* (2003*b*) relaminarization of a turbulent channel flow at $Re_\tau = 100$ was demonstrated and in Högberg & Henningson (2002) different transition scenarios were controlled in spatially developing boundary layer flows. Non-paralllel flows were also targeted in Cathalifaud & Bewley (2004*a*) Cathalifaud & Bewley (2004*b*) where the flow dynamics were modeled by the Parabolized stability equations (PSE).

The state feedback controller has showed to work well even for flows where nonlinear interactions take place we. However in real application the complete state information is seldom available. The full state information requirement can be relaxed through the use of a state estimator. The state estimator reconstructs the flow state based on wall measurements. The controller and estimator was combined into a compensator and tried in direct numerical simulations in Högberg *et al.* (2003*a*) but room for improvement in terms of the estimator efficiency.

The key to successful implementation of optimal control algorithms to engineering applications in the future is that appropriate sensors and actuators can be manufactured small and fast enough to target the small scales of turbulent

flows and to a low cost. The MEMS technology has been shown promising results but much work remains to be done, see e.g. Ho & Tai (1998) and Yoshino *et al.* (2003).

An overview of much of the most recent progress in the field of flow control is given in Kim (2003). Other recent reviews are given in e.g. Hinze & Kunish (2000), Bewley (2001), Högberg (2001).

1.3. Outline

In chapter 2 a linear optimal control problem is stated and the state feedback control and state estimation approaches used in order to solve the problem are discussed. Chapter 3 introduces the nonlinear optimization problem and presents a standard solution procedure that has been used in the present work. In both chapter 2 and chapter 3 some related results are shown. Chapter 4 gives a short description of the different flow solvers that have been used for the direct numerical simulations presented in this thesis. A summary and conclusions are given in chapter 5 which is followed by chapter 6 describing the different authors contributions to the papers presented in part two of the thesis.

CHAPTER 2

Linear control

The problem of linear model-based feedback control based on noisy measurements can be decomposed into two independent subproblems: first, the state feedback control problem also referred to as full information control, in which full state information is used to determine effective control feedback, and, second, the state estimation problem. In the state estimation problem wall measurements are continuously used to force a real-time calculation of the flow system in an optimal sense such that the calculated estimated flow state eventually approximates the actual flow state.

Once both subproblems are solved, one can combine them to control a flow based on noisy wall measurements of the flow system. The overall performance of the resulting linear feedback control scheme is limited by the individual performance of the two subproblems upon which it is based. For the application of linear control theory to wall-bounded flows, though encouraging results have been obtained previously on the state feedback control problem (see, for example, Bewley & Liu (1998) and Högberg *et al.* (2003*a*)), more effective state estimation strategies are needed.

In order to apply linear feedback control theory we need a linear system of equations describing the flow, an objective function which determines what the control should target, means of control, and models for the unknown disturbances acting on the flow.

The starting point when designing the state-feedback controller is the Orr–Sommerfeld/Squire equations which govern the evolution of small perturbations of the wall-normal velocity and wall-normal vorticity (v, η) in a laminar flow with the streamwise velocity component $U = U(y)$ and the spanwise velocity component $W = W(y)$. Control will be applied through blowing and suction distributed over the complete wall or on parts of the wall. Furthermore, only zero-mass flux control will be allowed since we primarily target the strong instabilities already in the flow with minute energy expenditure and not to adjust the mean flow. The Orr–Sommerfeld/Squire equations are

$$\begin{pmatrix} \dot{\hat{v}} \\ \dot{\hat{\eta}} \end{pmatrix} = \underbrace{\begin{pmatrix} \mathcal{L}_{OS} & 0 \\ \mathcal{L}_{C} & \mathcal{L}_{SQ} \end{pmatrix}}_{\mathcal{L}_{OSS}} \begin{pmatrix} \hat{v} \\ \hat{\eta} \end{pmatrix}, \tag{2.1}$$

where the Orr–Sommerfeld ($\mathcal{L}_{OS}$), the Squire ($\mathcal{L}_{SQ}$), and the coupling ($\mathcal{L}_C$) operators are

$$\begin{aligned}\mathcal{L}_{OS} &= \hat{\Delta}^{-1}[-i(k_xU + k_zW)\hat{\Delta} + ik_xU'' + ik_zW'' + \hat{\Delta}^2/Re],\\ \mathcal{L}_{SQ} &= -i(k_xU + k_zW) + \hat{\Delta}/Re,\\ \mathcal{L}_C &= i(k_xW' - k_zU'),\end{aligned} \tag{2.2}$$

and where $\{k_x, k_z\}$ is the wavenumber vector, $\hat{\Delta}$ denotes the horizontally Fourier transformed Laplacian and the wall-normal derivatives are indicated by $(')$. This system is accompanied by the following boundary conditions for the boundary layer flow

$$\begin{aligned}&\hat{v}(0,t) = \varphi, \quad D\hat{v}(0,t) \quad = 0, \quad \hat{\eta}(0,t) = 0,\\ &\hat{v}(y,t) = 0, \quad D\hat{v}(y,t) \quad = 0, \quad \hat{\eta}(y,t) = 0, \quad \text{as} \quad y \to \infty.\end{aligned} \tag{2.3}$$

The control enters the system through the boundary condition on the wall-normal velocity φ. The Reynolds number $Re_{\delta_0^*}$ is based on the freestream velocity and the displacement thickness at $x = 0$ denoted δ_0^*. For the channel flow configuration the freestream boundary condition is replaced by a no-slip condition identical to the lower wall boundary condition. In the channel flow the Reynolds number Re_{cl} is based in the centerline velocity and half-channel width h. Details regarding the linearization for the channel flow can be found in paper 1 and paper 2 and linearization in boundary layer flows can be found in paper 4.

2.1. Controller

In order to apply linear control theory to a dynamical system we need to put it on *state space form*

$$\begin{aligned}&\dot{q} = Aq + Bu + B_1 f, \quad q(0) = q_0,\\ &r = Cq + g,\end{aligned} \tag{2.4}$$

where q is the state. The external disturbances, denoted by f, force the state through the input operator B_1, and q_0 is the initial condition. The operator B_1 transforms a forcing on (u, v, w) to a forcing on (v, η). The control signal u affects the system through the input operator B. Operator C extracts the measurements from the state variable, and g adds a stochastic measurement noise with given statistical properties. The noisy measurement is then r. Once we have the physical model on this form, we can apply the tools from control theory, see for example Lewis & Syrmos (1995).

To fit the Orr–Sommerfeld/Squire equations with the accompanying boundary conditions we transform the blowing and suction boundary condition to a volume forcing. Since the system of equations is linear we can use the superposition principle and divide the flow in a homogeneous and a particular part. One valid solution to the particular problem is a stationary solution where the boundary condition is unity. This gives a system where the state q is defined

as

$$q = \begin{pmatrix} \hat{v}(y,t) \\ \hat{\eta}(y,t) \\ \varphi(t) \end{pmatrix}, \tag{2.5}$$

and operator A and B as

$$A = \begin{pmatrix} \mathcal{L}_{OSS} & 0 \\ 0 & 0 \end{pmatrix}, \quad B = \begin{pmatrix} -q_p \\ 1 \end{pmatrix}, \quad u = \dot{\varphi} \tag{2.6}$$

. We also define

$$\begin{pmatrix} \hat{v} \\ \hat{\eta} \end{pmatrix} = \begin{pmatrix} \hat{v}_h \\ \hat{\eta}_h \end{pmatrix} + \varphi \begin{pmatrix} \hat{v}_p \\ \hat{\eta}_p \end{pmatrix} = q_h + \varphi q_p. \tag{2.7}$$

Furthermore we are free to choose $\mathcal{L}_{OSS} q_p = 0$ which simplifies the system to solve.

The next step toward defining the optimization problem is to choose the objective function we want to minimize. In this study we have chosen to minimize the perturbation energy

$$J = \int_0^\infty (q^* \mathcal{Q} q + l^2 u^* u)\, \mathrm{d}t \tag{2.8}$$

where l^2 is included to penalize the time derivative of the control $\dot{\varphi}$

$$\mathcal{Q} = \begin{pmatrix} Q & Q q_p \\ q_p^* & (1+r^2) q_p^* Q q_p \end{pmatrix}, \tag{2.9}$$

where the term r^2 is an extra penalty on the control signal $\hat{\varphi}$, itself and where

$$\begin{pmatrix} \hat{v}^* & \hat{\eta}^* \end{pmatrix} Q \begin{pmatrix} \hat{v} \\ \hat{\eta} \end{pmatrix} = ||q||_E = \langle q, q \rangle_E = \frac{1}{8k^2} \int_{-1}^{1} \left(k^2 |\hat{v}|^2 + \left| \frac{\partial \hat{v}}{\partial y} \right|^2 + |\hat{\eta}|^2 \right) \mathrm{d}y, \tag{2.10}$$

is the kinetic energy of the flow perturbation where $k^2 = k_x^2 + k_z^2$. We now want to find the optimal $K(t)$ that feeds back the control based on the state q as

$$u = K(t) q. \tag{2.11}$$

A detailed derivation of the optimal feedback can be found in Lewis & Syrmos (1995). The lifting procedure as well as the complete derivation of the optimal controller can also be found in, for example, Högberg *et al.* (2003*a*) and Högberg (2001). The optimal feedback is given through the non-negative self-adjoint solution of a differential Riccati equation (DRE)

$$\frac{\partial X}{\partial t} + A^* X + X A - \frac{1}{\varepsilon} X B B^* X + Q = 0. \tag{2.12}$$

However to simplify the control problem we assume that $T \to \infty$ which means that the optimal feedback gain is computed for an infinite time horizon of the objective function. This gives us the algebraic Riccati equation (ARE)

$$A^* X + X A - \frac{1}{\varepsilon} X B B^* X + Q = 0 \tag{2.13}$$

where X again is the non-negative and self-adjoint solution. Note that the linear feedback law is the same regardless of what kind of disturbances that are present in the flow and is thus computed once and for all for a given base flow. From linear control theory it follows that the optimal choice of control gain K with respect to the chosen objective function is

$$K = -\frac{1}{l^2} B^* X. \tag{2.14}$$

The feedback gain K computed for a sufficient range of wavenumber pairs are then Fourier transformed in the horizontal directions gives us a physical space control law which was first reported in Högberg *et al.* (2003*a*).

2.2. Estimator

One of the primary challenges of the state estimation problem is that its framing is based centrally on quantities which are difficult to model, namely the expected statistics of the initial conditions, the sensor noise, and the external disturbances acting on the system. The state estimation problem may be thought of as a *filtering* problem; that is, the estimator uses the governing equation as a filter to extract, from the available noisy measurements of a small portion of the dynamic system, that component of the measurements which is most consistent with the dynamic equation itself. In other words, the estimator uses the governing equation to extract the signal from the noise, and in the process builds an estimate of the entire state of the system.

We now construct an estimator, analogous to system (2.4), of the form

$$\begin{aligned} \dot{\hat{q}} &= A\hat{q} + Bu - v, \quad \hat{q}(0) = 0, \\ \hat{r} &= C\hat{q}. \end{aligned} \tag{2.15}$$

The dynamic operator A and operator B are the same as in system (2.4). Added to this system is also a feedback forcing term v defined as

$$v = L\tilde{r} = L(r - \hat{r}), \tag{2.16}$$

proportional to the difference between the measurements of the flow and estimated flow. The feedback operator L is left to be specified and the choice is crucial for fast convergence of the estimator toward the actual flow.

Once we have supplied models for the statistical quantities of the initial condition q_0, the unknown external forcing f, and the unknown sensor noise g we can apply linear control theory to formulate and solve an optimization problem which gives an optimal L such that the estimator converges to a good approximation of q. The different statistical models we have chosen are briefly described in the following sections. More detailed descriptions of all the models are found paper 1. Paper 2 contains a detailed modeling of the external disturbances in a turbulent channel flow.

2.2.1. *Measurements*

The present work attempts to develop the best possible estimate of the state based on measurements of the flow on the wall(s). As discussed in paper 1, and in greater detail in Bewley & Protas (2004), the three measurements assumed to be available at the walls are the distributions of the streamwise and spanwise skin friction and pressure fluctuations.

$$\begin{cases} \tau_x = \tau_{xy}|_{\text{wall}} = \dfrac{1}{Re}\dfrac{\partial u}{\partial y}\bigg|_{\text{wall}} = \dfrac{1}{Re}\dfrac{i}{k^2}(k_x D^2 v - k_z D\eta)|_{\text{wall}}\,, \\ \tau_z = \tau_{zy}|_{\text{wall}} = \dfrac{1}{Re}\dfrac{\partial w}{\partial y}\bigg|_{\text{wall}} = \dfrac{1}{Re}\dfrac{i}{k^2}(k_z D^2 v + k_x D\eta)|_{\text{wall}}\,, \\ p = p|_{\text{wall}} = \dfrac{1}{Re}\dfrac{1}{k^2}D^3 v|_{\text{wall}}\,. \end{cases}$$

2.2.2. *Stochastic framework*

The flow system that we want to estimate is affected by an unknown initial condition, the unknown external disturbances that disturb the evolution of the state, and the unknown sensor noise that corrupts the measurements. Since the estimator is intended to converge effectively over a large number of possible realizations, a statistical description (mean and covariance) of these unknown quantities may be used to tune the feedback in the estimator design. The estimator which we will design, also known as a Kalman filter, will be optimal in the sense of obtaining the most accurate estimate possible over a large set of realizations of the system in which the initial conditions, external disturbances, and sensor noise have the assumed statistical properties.

In order to express the stochastic quantities we define the expectation operator $E[\cdot]$ as the average over all possible realizations of the stochastic input in question. In the present formulation it is the *covariance* that needs to be modeled carefully.

2.2.3. *Modeling of the initial condition*

The aim is to construct an estimator that works well for a range of possible initial conditions. We know however from flow physics that some initial conditions are more likely to appear. We thus construct a covariance model for the initial condition so that we can combine random modes with flow structures that we expect to appear, as for example Tollmien–Schlichting waves, streamwise vortices, or streaks depending on the specific flow conditions. The covariance of the initial condition is denoted S_0.

Note that the specific initial condition for each wavenumber pair $\{k_x, k_z\}$ is given only through its shape (of the coherent structures of the forcing) whereas amplitude and phase are random. Furthermore we assume that the mean of the initial condition is zero which means that there is no preferred structure. Due to the fact that the initial condition is always zero in the estimator S_0 also

represents the covariance of the state estimation error. Details on the modeling of the initial condition can be found in paper 1.

2.2.4. *Modeling of external disturbances in transitional flows*

We assume that the external disturbances $f = (f_1, f_2, f_3)^T$ in equation (2.4) is a zero-mean ($E[f_j(x, y, z, t)] = 0$) stationary white Gaussian process with auto-correlation

$$E[f_j(x, y, z, t) f_k(x + r_x, y', z + r_z, t')] = \underbrace{\delta(t - t')}_{\text{Temporal}} \underbrace{Q_{f_j f_k}(y, y', r_x, r_z)}_{\text{Spatial}}, \quad (2.17)$$

where $\delta(\cdot)$ denotes the Dirac δ-function. The derivation for the equations for the covariance of the state is simplified by the assumption of a white random process in time. This assumption is valid when the characteristic time scales of the external disturbances are short compared with the time scales of the flow system. When this is not the case an additional filter can be added that colors the external disturbances (see e.g. Lewis (1986)).

The corresponding quantity in Fourier space is the covariance operator $R_{f_i f_j}$ that we choose to model as

$$R_{f_j f_k}(y, y', k_x, k_z) = \delta_{jk} d(k_x, k_z) \mathcal{M}^y(y, y').$$

To formulate a useful model of $d = d(k_x, k_z)$ we want to parameterize it in such a way that the expected energy of the disturbances can easily be changed to fit different transition scenarios. For the boundary layer estimation presented in paper 4 the expected energy is assumed to decay exponentially in wavenumber space with the peak located at $\{k_x^0, k_z^0\}$

$$d(k_x, k_z) = \exp\left[-\left(\frac{k_x^0 - k_x}{d_x} \right)^2 - \left(\frac{k_z^0 - k_z}{d_z} \right)^2 \right],$$

with the additional design parameters d_x, and d_z. The design parameter d_y determines the width of the two-point correlation of the disturbance in the wall-normal direction according to

$$\mathcal{M}^y(y, y') = \exp\left[-\frac{(y - y')^2}{2 d_y} \right],$$

which means that we have localized structures in space.

In figure 2.1 examples of covariance models for both channel and boundary layer flows are presented. Figure 2.1(a) and 2.1(c) show examples on how $\delta_{jk} \mathcal{M}^y(y, y')$ varies with y and y' for $j = 1, 2, 3$ and $k = 1, 2, 3$ for channel and boundary layer flows respectively. The corresponding amplitude distribution as a function of wavenumber pair $\{k_x, k_z\}$ are shown in 2.1(b) and 2.1(d) for channel and boundary layer flows. The covariance model in Figure 2.1(d) is constructed to account for inflectional instabilities in a Falkner–Skan–Cooke boundary layer, see section 2.7.2. Note that other choices of d and $\mathcal{M}^y$ can be made which might be experimented with in future work.

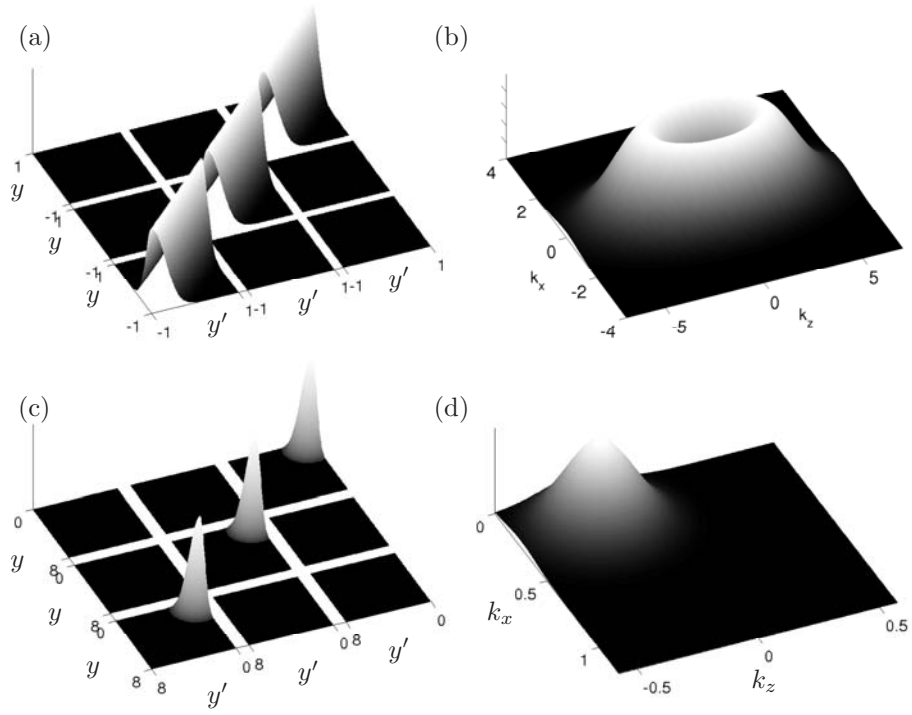

FIGURE 2.1. Statistical model for the external disturbances $R_{f_j f_k}(y, y', k_x, k_z) = \delta_{jk} d(k_x, k_z) \mathcal{M}^y(y, y')$ acting on system (2.4). (a) Example of the y-variation of $R_{f_j f_k}$ for channel flow. (b) Example of the amplitude d as a function of the wavenumber pair $\{k_x, k_z\}$ for channel flow. (c) The y-variation of $R_{f_j f_k}$ used for the estimation of cross-flow vortices in a FSC boundary layer flow. (d) The amplitude function for the same case as in (c). Note that the peak is translated to wavenumber pair $\{0.25, -0.25\}$ in order to sense the dominant eigenmode for this particular setup in an efficient manner.

2.2.5. *Modeling of external disturbances in turbulent flows*

A turbulent flow that has reached statistically steady state can be naturally fit into the framework of state feedback with time-independent feedback gains L. In the stochastic forcing vector f in equation (2.4) we now include the statistics of the nonlinear terms of the Navier–Stokes equations that are missing in the linear dynamic operator A. Jovanović & Bamieh (2001) proposed a stochastic disturbance model which, when used to force the linearized open-loop Navier–Stokes equation, led to a simulated flow state with certain second-order statistics (specifically, u_{rms}, v_{rms}, w_{rms}, and the Reynolds stress $-\overline{uv}$)

which to a certain degree matched statistics from DNS of a turbulent flow at $Re_\tau = 180$.

The system model considered in this work is the Navier–Stokes equation for the three velocity components $\{U, V, W\}$ and pressure P of an incompressible channel flow, written as a (nonlinear) perturbation about a base flow profile $\bar{u}(y)$ and bulk pressure variation $\bar{p}(x)$ such that, defining

$$\begin{pmatrix} U \\ V \\ W \\ P \end{pmatrix} = \begin{pmatrix} u \\ v \\ w \\ p \end{pmatrix} + \begin{pmatrix} \bar{u}(y) \\ 0 \\ 0 \\ \bar{p}(x) \end{pmatrix},$$

where $\{u, v, w, p\}$ denote the fluctuating components of the flow, we have

$$\frac{\partial u}{\partial t} + \bar{u}\frac{\partial u}{\partial x} + v\frac{\partial \bar{u}}{\partial y} = -\frac{\partial p}{\partial x} + \frac{1}{Re}\Delta u + f_1, \tag{2.18a}$$

$$\frac{\partial v}{\partial t} + \bar{u}\frac{\partial v}{\partial x} = -\frac{\partial p}{\partial y} + \frac{1}{Re}\Delta v + f_2, \tag{2.18b}$$

$$\frac{\partial w}{\partial t} + \bar{u}\frac{\partial w}{\partial x} = -\frac{\partial p}{\partial z} + \frac{1}{Re}\Delta w + f_3, \tag{2.18c}$$

$$\frac{\partial u}{\partial x} + \frac{\partial v}{\partial y} + \frac{\partial w}{\partial z} = 0, \tag{2.19}$$

where

$$\begin{aligned} f_1 &= -u\frac{\partial u}{\partial x} - v\frac{\partial u}{\partial y} - w\frac{\partial u}{\partial z} - \frac{\partial \bar{p}}{\partial x} + \frac{1}{Re}\frac{\partial^2 \bar{u}}{\partial y^2}, \\ f_2 &= -u\frac{\partial v}{\partial x} - v\frac{\partial v}{\partial y} - w\frac{\partial v}{\partial z}, \\ f_3 &= -u\frac{\partial w}{\partial x} - v\frac{\partial w}{\partial y} - w\frac{\partial w}{\partial z}. \end{aligned} \tag{2.20}$$

The base flow profile $\bar{u}(y)$ is defined as the mean flow,

$$\bar{u}(y) = \lim_{T\to\infty} \frac{1}{T\, L_x\, L_z} \int_0^T \int_0^{L_x} \int_0^{L_z} U \,\mathrm{d}z \,\mathrm{d}x \,\mathrm{d}t,$$

and $\bar{p}(x)$ is selected to account for the mean pressure gradient sustaining the flow.

We will assume that $f = (f_1, f_2, f_3)^T$ is essentially uncorrelated from one time step to the next (that is, we assume that f is "white" in time) in order to simplify the design of the estimator. We proceed by developing an accurate model for the assumed spatial correlations of f. As the system under consideration is statistically homogeneous in the x- and z-directions, the covariance of the stochastic forcing f may be parameterized in physical space as in (2.17).

The statistics of f is gathered in direct numerical simulations of turbulent channel flow at Reynolds number $Re_\tau = 100$. As the system under consideration is statistically homogeneous, or "spatially invariant", in the x- and z-directions, it is more convenient to work with the Fourier transform of the two-point correlation $Q_{f_i f_j}$ rather than working with $Q_{f_i f_j}$ itself, as the calculation of $Q_{f_i f_j}$ in physical space involves a convolution sum, which reduces to a simple multiplication in Fourier space. The Fourier transform of $Q_{f_i f_j}$, which we identify as the spectral density function $R_{f_i f_j}$, is defined as

$$R_{f_i f_j}(y, y', k_x, k_z) = \frac{1}{4\pi^2} \int_{-L_x/2}^{L_x/2} \int_{-L_z/2}^{L_z/2} Q_{f_i f_j}(y, y', r_x, r_z) \exp[-ik_x r_x - ik_z r_z] \, \mathrm{d}r_x \mathrm{d}r_z. \tag{2.21}$$

Note that we neglect correlations between different wavenumber pairs as this is not needed the way we build the estimator. The spectral density function can thus be written

$$R_{f_i f_j}(y, y', k_x, k_z) = \lim_{T \to \infty} \frac{1}{T} \int_0^T f_i(k_x, y, k_z) f_j^*(k_x, y', k_z) \, \mathrm{d}t. \tag{2.22}$$

For each wavenumber pair $\{k_x, k_z\}$ we now have a matrix of covariance data $R_{f_i f_j} = R_{f_i f_j}(y, y', k_x, k_z)$ which can be seen for different wavenumber pairs in figure 2.2. The data is then used in the optimization problem when computing the feedback gains. The resulting estimation gains are well resolved for the range of wavenumber pairs used in the DNS. The gains transformed to physical space convolution kernels are shown in figure 2.3 for the v (left column) and η (right column) components of the flow and for the three measurements τ_x, τ_z, and p. The maximum amplitude as a function of wavenumber pair $\{k_x, k_z\}$ is shown in figure 2.4.

All turbulent direct numerical simulations are performed with the code briefly described in chapter 4 and more thoroughly in paper 2.

2.2.6. *Modeling of sensor noise*

All three wall measurements described in section 2.2.1 are assumed to be corrupted by sensor noise. The noise for each sensor is modeled as a random process, white in both space and time, and where the amplitude determines the quality of each sensor. The measurements are also assumed to be independent of each other. The covariance of the noise vector g, appearing in system (2.4), can thus be described in Fourier space by a diagonal 3×3 matrix G whose diagonal elements α_ι^2 are the variances of the individual sensor noise.

When the signal-to-noise ratio is low the measured signal should be fed back gently into the estimator. If the signal-to-noise ratio is high we trust the signal and thus it can be fed back with more strength.

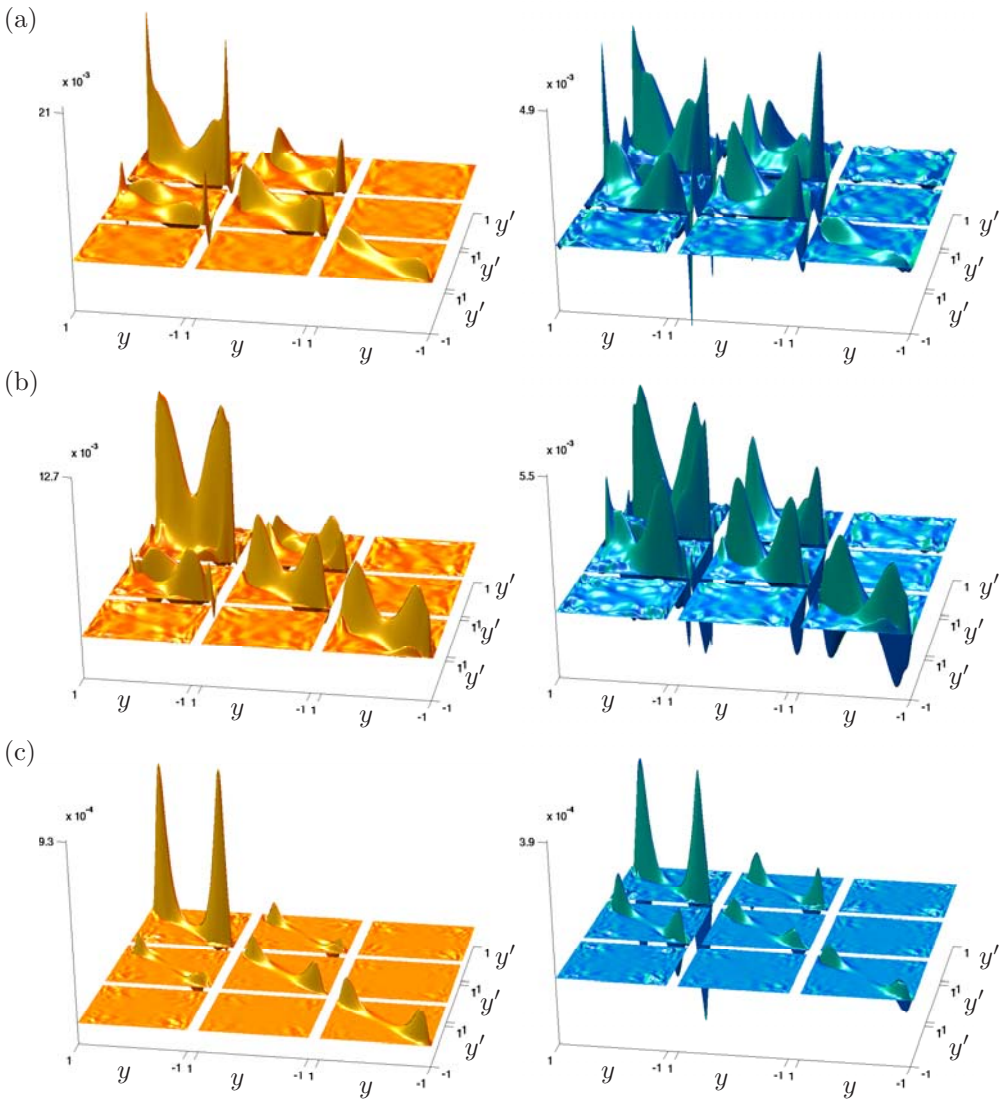

FIGURE 2.2. The covariance of $\hat{f}$, taken from DNS, at wavenumber pair $\{0.5, 1.5\}$, $\{3, 1.5\}$, and $\{10, 30\}$ in figure (a), (b), and (c) respectively. The nine "squares" correspond to the correlation between the different components of the forcing vector. From top to bottom and left to right the components are f_1, f_2, and f_3 on each axis. The width of each side of each square represents the width of the channel, $[-1, 1]$. The variance is seen along the diagonal of each square. The left column contains the real part and the right column represents the imaginary part.

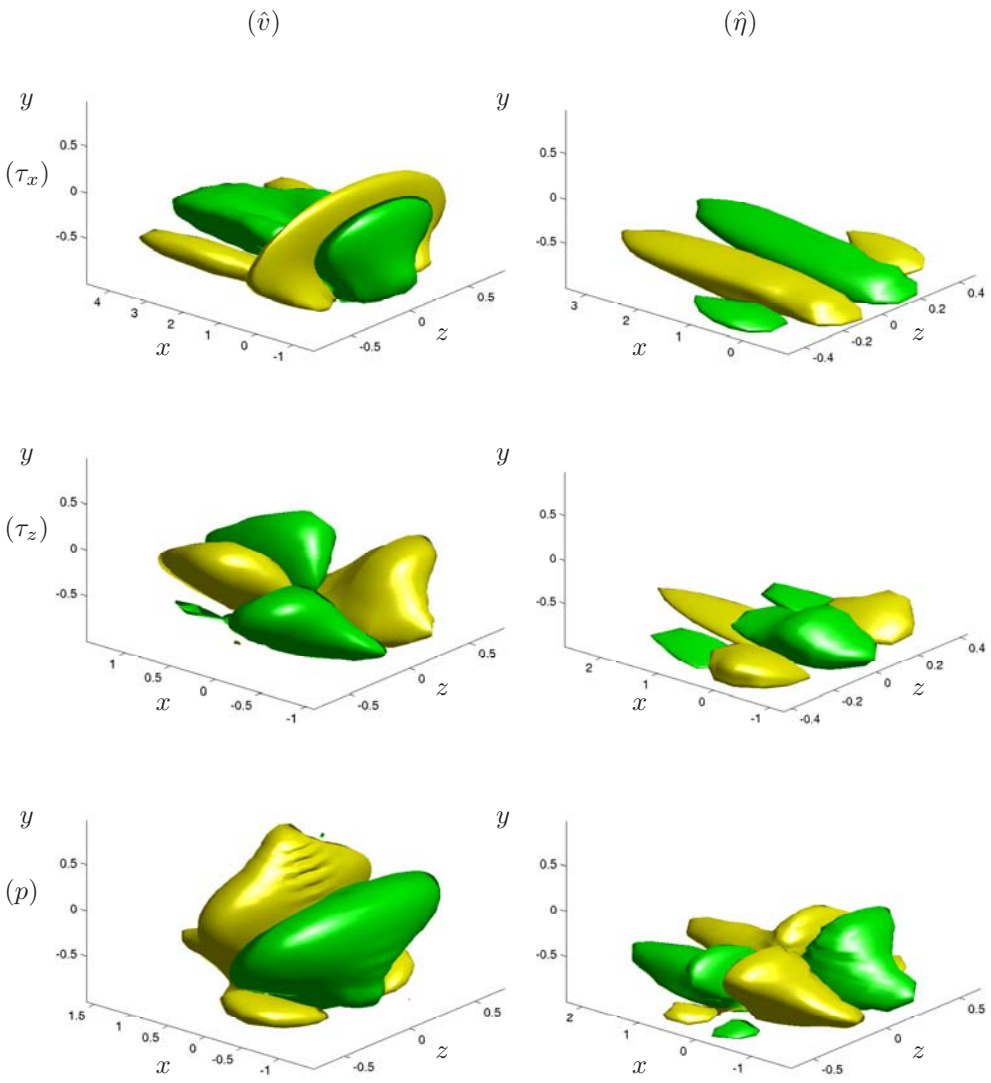

FIGURE 2.3. Isosurface plots of steady-state estimation convolution kernels relating the measurements τ_x, τ_z, and p at the point $\{x = 0,\ y = 0,\ z = 0\}$ on the wall to the estimator forcing on the interior of the domain for the evolution equation for the estimate of (left) $\hat{v}$ and (right) $\hat{\eta}$. Positive (green) and negative (yellow) isosurfaces with isovalues of $\pm 5\%$ of the maximum amplitude for each kernel are illustrated. The kernels are based on statistical data gathered from turbulent direct numerical simulations.

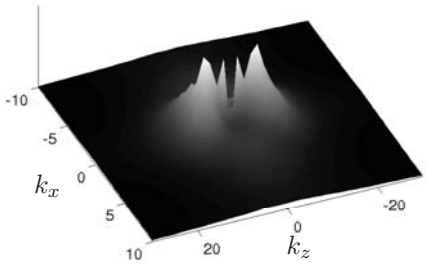

FIGURE 2.4. Maximum amplitude of turbulent covariance data as a function of wavenumber pair $\{k_x, k_z\}$. The corresponding two-point correlations along the wall-normal coordinate are shown in figure 2.2.

For transitional flows an intermediate level of feedback is desired in the estimator design due to the fact that if the feedback becomes too strong it may knock the estimated flow out of the small perturbation neighborhood assumed in the linear model used in the design process. On the other hand if it becomes to weak the convergence in the estimator may be both slow and inaccurate. For given covariances of the initial conditions and external disturbances we thus have the means, through the sensor noise, to tune the feedback strength into the estimator.

2.2.7. *Kalman filter*

Kalman filter theory, combined with the models outlined in sections 2.2.3, 2.2.4, and 2.2.6 for the statistics of the unknown initial conditions q_0, the unknown external forcing f, and the unknown sensor noise g respectively, provides a convenient and mathematically-rigorous tool for computing the feedback operator L in the estimator described above such that $\hat{q}$ converges to an accurate approximation of q. Note that the volume forcing v used to apply corrections to the estimator is proportional to the measurement error $\tilde{r} = r - \hat{r}$.

The solution of the Kalman filter problem in the classical, finite-dimensional setting is well known (see, e.g., Lewis & Syrmos (1995) p. 463–470). The corresponding operator equations applicable here, though more involved to derive, are completely analogous (see Balakrishnan 1976).

From linear control theory is follows that the covariance $S(t) = R_{qq}(t)$ of the flow state $q(t)$ is governed by the Lyapunov equation

$$\dot{S}(t) = AS(t) + S(t)A^* + BRB^*, \quad S(0) = S_0. \tag{2.23}$$

The covariance $P(t) = R_{\tilde{q}\tilde{q}}(t)$ of the state estimation error $\tilde{q}(t) = q(t) - \hat{q}(t)$, for a given $L(t)$, is governed by the Lyapunov equation

$$\dot{P}(t) = A_0(t)P(t) + P(t)A_0^*(t) + BRB^* + L(t)GL^*(t), \quad P(0) = S_0, \quad (2.24)$$

where $A_0(t) = A + L(t)C$. The optimal $L(t)$ that minimizes the expected energy of the state estimation error at all times (that is, which minimizes the trace of $P(t)$) is given by the solution of the differential Riccati equation (DRE)

$$\dot{P}(t) = AP(t) + P(t)A^* + BRB^* - P(t)C^*G^{-1}CP(t), \quad P(0) = S_0, \quad (2.25)$$

where

$$L(t) = -P(t)C^*G^{-1}. \quad (2.26)$$

Note that the expressions in equations (2.23), (2.24), and (2.25) are identical in both the finite-dimensional and infinite-dimensional settings.

Note also that, for a linear, time-invariant (LTI) system (that is, for A, B, C, R, G independent of time), the covariance of the estimation error, $P(t)$, and the corresponding feedback which minimizes its trace, $L(t)$, follow a transient near $t = 0$ due to the effect of the initial condition S_0, eventually reaching a steady state for large t in which $\dot{P}(t) = 0$ and $\dot{L}(t) = 0$. In order to minimize the magnitude of the transient of the trace of $P(t)$, it is necessary to solve the differential Riccati equation given above. If one is only interested in minimizing the trace of $P(t)$ at statistical steady state, it is sufficient to compute time-independent feedback L by solving the algebraic Riccati equation (ARE) formed by setting $\dot{P}(t) = 0$ in (2.25).

2.2.8. *Extended Kalman filter*

The Kalman filter is an "optimal" estimator (in several rigorous respects—see Anderson & Moore (1979) for a detailed discussion) in the linear setting. When a Kalman filter is applied to a nonlinear system, its performance is typically degraded, due to the fact that the linear model upon which the Kalman filter is based does not include all the terms of the (nonlinear) equation governing the actual system. A common approach to partially account for this deficiency is to reintroduce the system nonlinearity to the estimator model after the Kalman filter is designed. This approach is called an extended Kalman filter, see e.g. Gelb (1974). This type of estimator is identical to the Kalman filter except that the nonlinearity in the system is also present in the estimator model when marching in time. The extension makes some sense: if the estimate of the state happens to match the actual state, no feedback from measurements is required for the extended Kalman filter to track the subsequent flow state. This is not the case for the standard (linear) Kalman filter.

2.3. Compensator

The compensator combines the full information controller described in section 2.1 with the state estimator described in section 2.2 in the sense that the estimated flow state in the estimator is fed into the controller. Since the estimator

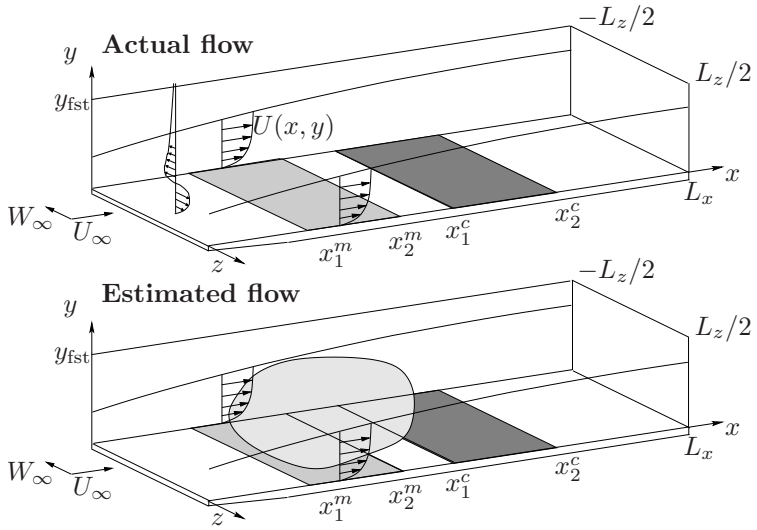

FIGURE 2.5. Compensator configuration. The upper box represents the "real" flow where the light grey rectangle along the wall is the measurement region and the corresponding dark grey rectangle is the control area. In the beginning of the box a perturbation is indicated as a function of the wall-normal coordinate. This perturbation will evolve as we integrate the system in time. The estimated flow system is depicted in the lower box. Here the volume force that is based on the wall measurements and the estimation gains is shown as a grey cloud in the computational domain.

only relies on different measurements of flow quantities at the wall the requirement of complete flow information to compute a control is relaxed which closes the gap to experimental realization of the control algorithm. Note however that instead a real-time calculation of the estimator flow system has to be done.

The compensator algorithm is depicted in figure 2.5. The "real" flow could be an experimental setup where only wall information is extracted. However, so far in our studies the "real" flow has always been a computer simulation. The algorithm can be summarized in the following steps:

1. Extract wall measurements in both "real" and estimated flow
2. Compute the estimator volume forcing based on precomputed estimation gains and the difference of the wall measurements from the "real" and estimated flow
3. Apply the volume forcing to the estimator flow to make it converge to the "real" flow
4. Compute control signal based on the reconstructed state in the estimator
5. Apply the control signal in both the "real" and estimated flow

2.4. Numerics

In order to compute the optimal control and feedback gains from the ARE or the DRE, it is necessary to discretize the operator form of the equations (2.13) and (2.25) and solve them in the finite-dimensional setting. However, in order to be relevant for the PDE problem of interest, the resulting feedback gains must converge to continuous functions as the numerical grid is refined.

2.4.1. *Spatial discretization*

We need to build discrete system operators for A, B, B_1, C, their respective adjoints as well as the energy measure Q in the objective function and the disturbance covariances R, G, and S_0. In all our studies, the discrete operators are obtained through enforcement of the Orr–Sommerfeld/Squire equations at each point of a Gauss–Lobatto grid using a Chebyshev collocation scheme, taking

$$f_i = f(y_i), \quad y_i = \cos\frac{i\pi}{N}, \quad i = 0, \ldots, N,$$

where $N + 1$ is the number of grid points in the wall-normal direction. The discrete operators and differentiation matrices are determined using the spectral Matlab Differentiation Matrix Suite of Weideman & Reddy (2000). This suite provides differentiation matrices invoking clamped boundary conditions ($f(\pm 1) = f'(\pm 1) = 0$), using the procedure suggested by Huang & Sloan (1993), to give an Orr–Sommerfeld/Squire matrix with satisfactory numerical properties, avoiding unstable or lightly-damped spurious eigenmodes. The first-order, second-order, and third-order differentiation matrices so obtained, denoted D^1, D^2, and D^3 respectively, are combined according to the equations given previously to compute the discrete matrices A, B, and C in a straightforward fashion.

Necessary adjoint operators are defined in a discrete sense meaning that they are the conjugate transpose of the operator itself. The integration weights $\mathsf{W}(y_j)$ for the Chebyshev grid with the Gauss–Lobatto collocation points are computed using the algorithm from Hanifi *et al.* (1996). These weights provide spectral accuracy in the numerical integration used to assemble the energy measure matrix Q.

2.4.2. *Temporal discretization*

When searching for the infinite time horizon control feedback or the estimation feedback for statistically steady state we only solve the ARE defined in equation (2.13). However, in paper 1 we also solve the time evolution of the estimation feedback gains which requires the solution of the DRE defined as in equation (2.25). One could directly march the DRE in time with, for example, a Runge–Kutta method but instead we choose to march in time the Chandrasekhar equation, see Kailath (1973), which solves for the time derivative of the estimation error covariance matrix, $\dot{\mathsf{P}}(t)$. More details about the algorithm are found in paper 1.

2.5. Transitional channel flow estimation

The stochastic models that are developed in paper 1, and briefly discussed in section 2.2, are used to estimate infinitesimal as well as finite amplitude perturbations in direct numerical simulations of a channel flow at $Re_{cl} = 3000$ based on the centerline velocity and channel half width. The localized flow perturbations studied in Henningson *et al.* (1993) are used to test the convergence of the estimator.

The evolution of the energy of the state and estimation error for both the moderate-amplitude and the small-amplitude perturbations are plotted in figure 2.6. All curves have been normalized to unity at $t = 0$ to ease the comparison. The difference in normalized energy between the two cases is due to nonlinear interactions that take place in the moderate-amplitude case (compare the thick solid line and the thick dashed line). For both cases, the initial stage of the evolution (during which nonlinear effects are fairly small) is well estimated (thin lines). As the moderate-amplitude perturbation evolves and its amplitude grows, nonlinear effects become significant, and the performance of the linear estimator (thin solid line) is degraded as compared with the performance of the linear estimator in the small-amplitude case (thin dashed line), but still it is relatively good when compared to the flow energy.

By using an extended Kalman filter, as described in section 2.2.8, the performance of estimator is improved when nonlinear interactions are present in the flow to be estimated. This can be clearly seen in figure 2.6 where the extended Kalman filter (thin dot-dashed line) is performing better than its standard Kalman filter counterpart (the thin solid line) .

For these cases nine different set of estimation gains have been applied which are the optimal gains at the times given in the following sequence $\{1, 2, 3, 4, 5, 10, 15, 20, 60\}$. This sequence captures the fast initial transient in the gains and converges to the steady state gains.

2.6. Turbulent channel flow estimation

By using statistics of nonlinear terms in the Navier–Stokes equations, as outlined in paper 2, into the state feedback optimization problem we can compute well-resolved estimation gains for all three wall-measurements defined defined in section 2.2.1. Here we have chosen to define the measurement vector r to contain scaled versions of the wall values of the wall-normal derivative of the wall-normal vorticity, η_y/Re, the second wall-normal derivative of the wall-normal velocity, v_{yy}/Re, and the pressure, p. Note that we can easily relate this transformed measurement vector to the raw measurements of $\tau_x = u_y/Re$, $\tau_z = w_y/Re$, and p on the walls, which might be available from an experiment.

The resulting physical-space convolution kernels, shown in section 2.2.5, are then used to estimate a turbulent channel flow at $Re_\tau = 100$ with both Kalman and extended Kalman filters. In order to tune the available estimator parameters the Reynolds number was kept low to ease the resolution requirements and hence the computational effort for the simulations.

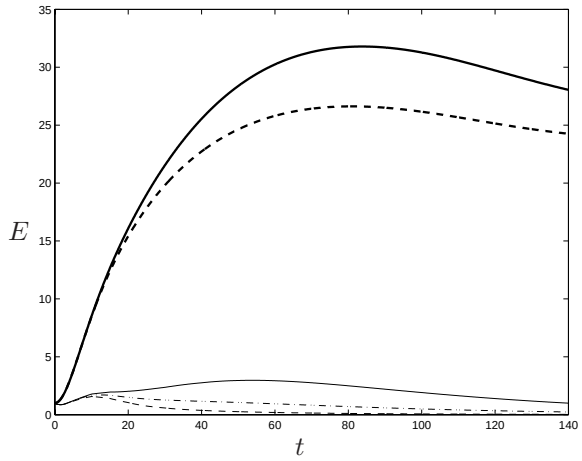

FIGURE 2.6. Evolution of the normalized flow energy (thick lines) and normalized estimation error energy (thin lines) for the case with moderate-amplitude initial conditions (solid) and low-amplitude initial conditions (dashed). The evolution of the normalized estimation error energy for the extended Kalman filter in the case with moderate-amplitude initial conditions is also plotted (thin dot-dashed line), illustrating a significant improvement as compared with the performance of the corresponding Kalman filter (thin solid line) when nonlinearities are significant.

In figure 2.4 the total energy of the estimation error, defined as

$$\mathrm{errn}_y^{\mathrm{tot}}(q,\hat{q}) = \frac{\left(\int_0^{L_x}\int_0^{L_z}(\hat{q}-q)^* Q(\hat{q}-q)\,\mathrm{d}x\mathrm{d}z\right)^{1/2}}{\left(\int_0^{L_x}\int_0^{L_z} q^* Q q\,\mathrm{d}x\mathrm{d}z\right)^{1/2}}, \tag{2.27}$$

is plotted versus the wall-normal coordinate. The actual and estimated state are denoted by q and $\hat{q}$ respectively. This is the quantity that we, in an average sense, are minimizing for in the construction of the optimal estimation gains which makes it a relevant measure when evaluating the performance of the estimator. Note that operator Q represent the energy inner-product in (v,η) coordinates as defined in (2.10). Close to the wall the error is small but it increases as we go further into the channel. The thin and thick lines are from Kalman and extended Kalman filter simulations respectively. To further investigate the impact of using estimation gains based on the statistics from the present study or based on simpler models such as assuming spatially uncorrelated stochastic forcing we also test the estimator performance (shown as dashed lines) for only one measurement. Based on a spatially uncorrelated stochastic model and the numerical approach presented in section 2.4.1 it is not

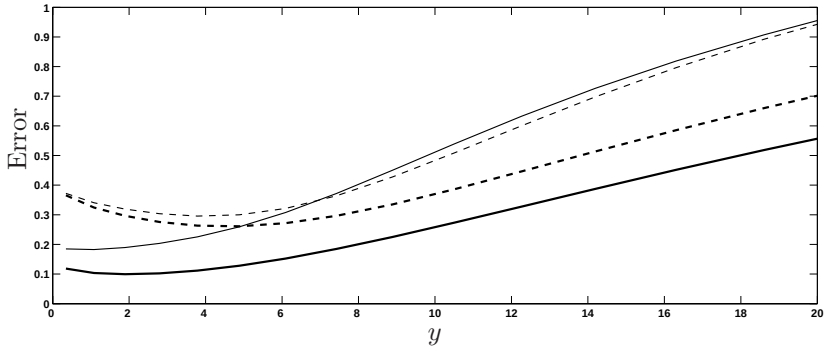

FIGURE 2.7. The total energy of the estimation error is shown as a function of the wall-normal distance. The solid line denotes the error when all three measurements are applied in the estimator. The dashed line represents the estimator performance when using only the η_y measurement respectively. The thick lines show the extended Kalman filter and the thin lines the Kalman filter data.

possible to retrieve well-resolved gains for more than one measurement. The major difference however comes from the fact that we now have estimation gains for all three measurements which can be seen as the solid lines in figure 2.7. Despite the strong nonlinear interactions in the turbulent flow the Kalman filter is performing surprisingly well compared to the extended Kalman filter.

2.7. Compensator results

A summary of the compensator results from paper 4 are discussed in the following section. For details about box sizes and resolutions and the numerical parameters for the different disturbances see paper 4. The code used for the compensator simulations are described in chapter 4.

Note, that in the work with compensators in spatially developing boundary layers so far we let the estimator run for a while before we turn on the controller. Once the estimator has converged we turn on the controller and we thereby close the loop in figure1 2.5. This is done to give the controller better initial state information. Note also that we let all perturbation types evolve long enough so that they have propagated through the computational box before we turn in the control. In future studies we will explore the limits of the compensator in terms of how much information the controller needs in the initial transient phase.

2.7.1. *Parallel Falkner–Skan–Cooke boundary layer*

To verify the compensator algorithm in the DNS code we tested it in a parallel Falkner–Skan–Cooke (FSC) boundary layer flow with low-amplitude disturbances. The base flow considered has a Reynolds number $Re_{\delta_0^*} = 337.9$ based on

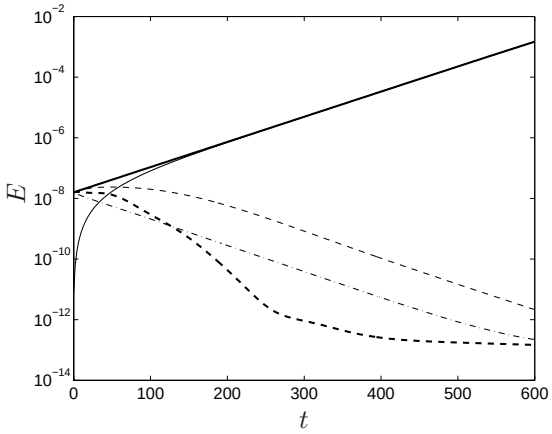

FIGURE 2.8. Time evolution of the perturbation energy of the uncontrolled unstable eigenmode at $\alpha = 0.25, \beta = -0.25$ in a Falkner–Skan–Cooke boundary layer and the corresponding controlled system. Solid: uncontrolled energy growth. Dashed: full information control is applied. Solid-thin: energy growth in the estimator when no control is applied. Dash-dotted-thin: the estimation error when no control is applied. Dashed-thin: compensator control is applied.

the displacement thickness, δ_0^*, and chordwise freestream at the beginning of the computational box. There is also a spanwise velocity component $W_\infty = 1.442$ of the base flow normalized with the chordwise freestream velocity. The initial condition is perturbed with an unstable eigenmode at wavenumber pair $\{k_x = 0.25, k_z = -0.25\}$. Due to an inflection point in the base flow this eigenmode grows exponentially in time as can be seen in figure 2.8. Both the full information controller and the compensator control are able to switch the exponential disturbance growth into decay. Since the initial condition in the estimator is the base flow without any perturbations the compensator performance is not as good as the full-state information in the beginning. Once the estimate gets closer to the real flow the disturbance is decaying exponentially when compensator control is applied.

2.7.2. *Spatially developing Falkner–Skan–Cooke boundary layer*

The same base flow setup as described in section 2.7.1 is used here with the only difference that the flow is now developing downstream. A perturbation with random spanwise distribution and randomly varying amplitudes develop into traveling cross-flow vortices downstream.

The measurement region is located in $x \in [40, 150]$ and the control is applied in the strip $x \in [175, 325]$. In figure 2.9 the time averaged perturbation energy as a function of the chordwise coordinate and integrated in the spanwise

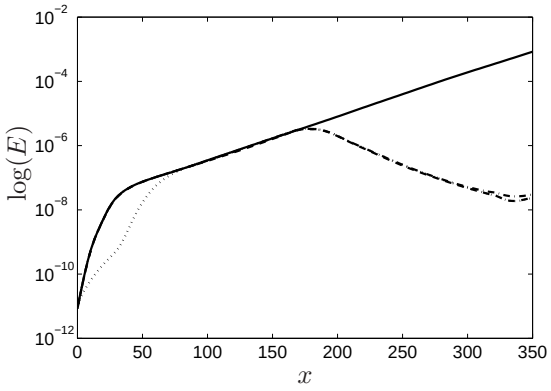

FIGURE 2.9. Time averaged perturbation energy for cross-flow vortices in a spatial Falkner–Skan–Cooke boundary layer. Solid: uncontrolled energy growth. Dashed: full information control. Dash-dotted: energy growth and decay when compensator control is applied.

direction is plotted for uncontrolled flow (solid) and full information control (dashed) and compensator control (dash-dotted).

The perturbation energy in the estimator is shown as a dotted line. As can be seen in the figure the performance of the two controllers are similar. The compensator control is only slightly less efficient in reducing the perturbation energy than the full information controller and they both turn exponential growth in to decay. In figure 2.10(a) and (b) the wall-normal velocity component is shown in a x–z plane at $y = 0.5$ for uncontrolled and compensator controlled flow respectively. At the beginning of the control region, the control is of opposition type since the light and dark regions are shifted over the control domain.

Figure 2.11 shows the evolution of disturbance energy integrated in space. During the first 2000 time units the "real" flow is run in parallel with the estimator to let the estimator catch up. After about 500 time units the estimated state has converged to the actual flow downstream of the measurement region. At $t = 2000$ the compensator control is turned on and the disturbance energy starts to decay.

2.7.3. *Tollmien–Schlichting waves in a Blasius boundary layer*

The Tollmien–Schlichting (TS) wave perturbation is applied and studied in a Blasius boundary layer with zero streamwise pressure gradient. We also assume no mean-flow component in the z-direction. The wave is introduced by applying an oscillating volume force localized in the x- and z-direction in the far upstream part of the computational box. The dimensionless oscillating frequency is $F = 200$ where $F = 10^6 2\pi f\nu/U_\infty^2$ and where f is the frequency

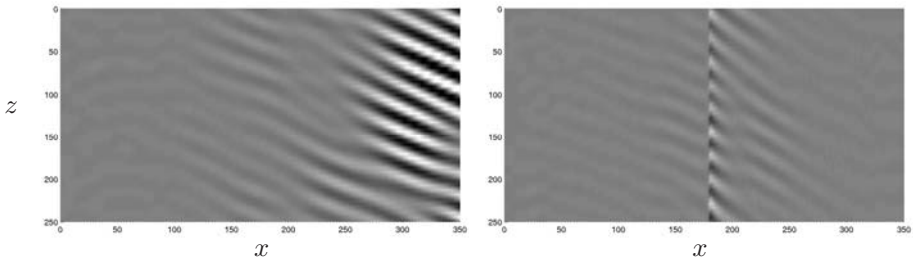

FIGURE 2.10. Snapshots of the wall-normal velocity component at $y = 0.5$. The flow state is depicted in part (a). In (b) the effect of the compensator control is shown. In the controlled flow the control has been applied for 2000 time units i.e. all the transient effects that occur due to the startup of the control with the perturbations present have settled down. The control is applied in $x \in [175, 325]$. The black to white scale lies in the interval $v \in (-0.00045, 0.00045)$.

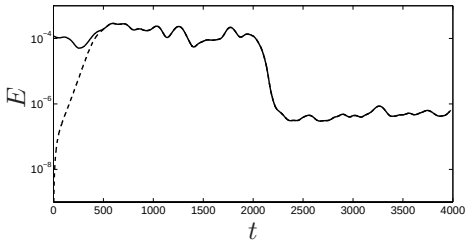

FIGURE 2.11. *Time evolution* of the disturbance energy integrated throughout the computational box. During the first 2000 time units the flow is uncontrolled. At time $t = 2000$ the compensator control is turned on. Solid: energy in the "real" flow. Dashed: energy in the estimator.

and ν is the kinematic viscosity. Branch I for this TS-wave is located at $x = 27$ and extends to branch II at $x = 219$. The measurement region is $x \in [40, 150]$ and the control region is $x \in [175, 325]$ which means that they both overlap the exponential growth region between branch I and branch II.

In figure 2.12 the uncontrolled energy growth and decay is plotted as a solid line. The volume forcing does not impose a clean TS-wave from the beginning which explains the initial transient and but further downstream a TS-wave is emerging and we get the expected exponential growth. The dashed and dash-dotted lines show the energy growth which is soon turned into decay in the beginning of the control region when the full information and compensator control are applied. The difference between the full information control and compensator control is due to the approximative flow state from the estimator the compensator control is based on. However, despite the approximative flow

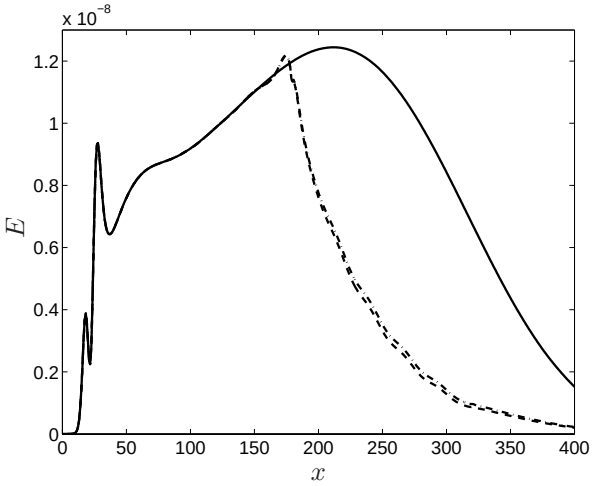

FIGURE 2.12. Spatial evolution of the perturbation energy of a TS-wave in a spatially growing boundary layer. Solid: uncontrolled energy growth. Dashed: energy growth and decay when full information control is applied. Dash-dotted: energy growth and decay with compensator control.

state information the compensator is are able to turn the exponential growth into exponential decay.

2.7.4. *Streamwise streaks in a Blasius boundary layer*

A transient growth scenario is studied where optimal perturbations are developing downstream to form streamwise streaks. The spatial optimal perturbation (see Andersson *et al.* (1999) and Luchini (2000)) with maximum growth at $x = 237$ is introduced in the fringe region.

The measurement region is located in $x \in [0, 300]$ and the control is applied in two different simulations at $x \in [300, 450]$ and $x \in [300, 750]$ respectively. In figure 2.13 the disturbance energy integrated in time and spanwise direction, is shown. Both the full information control (dashed) and the compensator control (dash-dotted) equally well manage to lower the disturbance amplitude over the control strip. The longer interval is shown with thin lines and the short interval is represented with thick lines. Right behind both the control strips however there is a stronger dip for the full information controller. Eventually the disturbance energy starts to increase again but without reaching the amplitude levels for the uncontrolled flow. Note that the gains are computed for a flow linearized around the same streamwise position at $x = 375$.

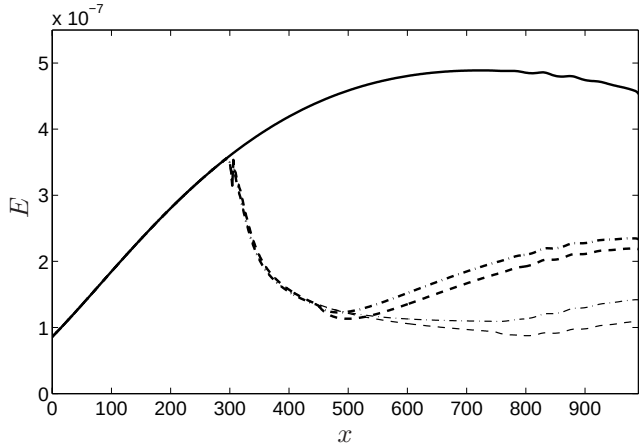

FIGURE 2.13. The energy of the optimal spatial perturbation at $x = 237.24$ as a function of downstream position. Solid: uncontrolled energy growth. Dashed: full information control applied in region $x \in [300, 450]$. Dash-dotted: compensator control with the measurement region $x \in [0, 300]$ and the control region $x \in [300, 450]$. Thin-solid: estimator energy. Thin-dashed: full information control applied in region $x \in [300, 725]$. Thin dash-dotted: compensator control with the measurement region $x \in [0, 300]$ and the control region $x \in [300, 725]$.

CHAPTER 3

Nonlinear control

The goal of an optimal controller is to minimize or maximize an objective function. When formulating such a problem, three important decisions are needed, governing equations, an objective function to determine what we want to control, and means of control. For a particular flow geometry with given fluid properties, each choice has to be made with care. The state equation should of course model the appropriate physics. This choice also indirectly affects the choice of methods to use when solving the optimal control problem. If we are working with nonlinear governing equations, such as the Navier–Stokes equations, we have to use an iterative procedure to solve the optimization problem and retrieve the optimal control, as opposed to the linear controller which can be applied online in a feedback loop. This is further described in chapter 2. In this chapter two different nonlinear optimization problems are stated, solution strategies are described and some results are presented. In terms of nonlinear control the main effort has been directed toward finding optimal blowing and suction profiles in boundary layer flows. An initial study to find optimal initial conditions is also described. The complete descriptions of the nonlinear optimization studies are found in paper 5.

3.1. Governing equations

3.1.1. *Blowing and suction control*

The governing equations are the incompressible Navier–Stokes equations, here written on dimensionless form,

$$\begin{cases} \dfrac{\partial u}{\partial t} + (u \cdot \nabla)u = -\nabla\pi + \dfrac{1}{Re}\Delta u, \\ \nabla \cdot u = 0, \\ u|_{t=0} = u_0, \end{cases} \tag{3.1}$$

where $u = (u_1, v, w)$ is the velocity vector and π is the pressure. Periodic boundary conditions in x- and z-directions, and control through blowing and suction together with a no-slip condition for the directions parallel to the wall gives the complete set of boundary conditions. The numerical scheme is further described in chapter 4.

To get the desired effect out of the control one needs to choose what properties of the flow to target. This choice is formulated as an *objective function*

which in this particular case has the form

$$J(\varphi) = \frac{\varepsilon}{2} \int_{T_1^c}^{T_2^c} \int_{\Gamma} |v|^2 \, \mathrm{d}\Gamma \, \mathrm{d}t + \frac{1}{2} \int_{T_1^o}^{T_2^o} \int_{\Omega} |u - u_T|^2 \, \mathrm{d}Q, \tag{3.2}$$

where (T_1^c, T_2^c) is the control time period and (T_1^o, T_2^o) is the observation time period. The target velocity profile is denoted by u_T and the control, which is the wall-normal velocity on the wall, is denoted by v. A regularization term with penalty parameter ε is also added to put a limit on the control strength. The choice of objective function is usually a non-trivial matter due to the complicated physics present in aerodynamic flows.

3.1.2. *Initial condition control*

The derivation and implementation of finding the optimal initial condition that gives the highest energy amplification is done for channel flows. The non-dimensional, incompressible Navier–Stokes equations with Reynolds number, Re, based on the centerline velocity and half the channel height are,

$$\begin{cases} \dfrac{\partial u}{\partial t} + (u \cdot \nabla)u - \dfrac{1}{Re}\Delta u + \nabla \pi = -\nabla P, \\ \nabla \cdot u = 0, \\ u|_{t=0} = \varphi + u_T(0), \end{cases} \tag{3.3}$$

where $u = (u_1, v, w)$ is the velocity vector, π is the pressure and ∇P represents the pressure gradient driving the flow and can either be constant or used to ensure constant mass flux. The control φ is entering the equations through the initial condition as a disturbance on top of a laminar flow. Periodic boundary conditions are assumed in the x- and z-directions and no-slip conditions for the directions parallel to the walls.

The objective function J measures the ratio in disturbance energy at final and initial time

$$J(\varphi) = -\frac{\displaystyle\int_{\Omega} |u(T) - u_T(T)|^2 \, \mathrm{d}\Omega}{\displaystyle\int_{\Omega} |\varphi|^2 \, \mathrm{d}\Omega}. \tag{3.4}$$

Time T denotes the final simulation time. The target velocity profile denoted u_T represents the laminar flow field.

3.2. Nonlinear optimization problem and the gradient

Once the objective functions (3.2) and (3.4) are defined we can formulate the nonlinear optimization problem as: find φ^* which satisfies

$$J(\varphi^*) \leq J(\varphi) \quad \forall \ \varphi \in \mathcal{U}_{\mathrm{ad}} \tag{3.5}$$

where $\mathcal{U}_{ad}$ has been used to denote the set of *admissible controls*.

To solve the nonlinear optimization problem (3.5) we use a gradient based approach. The gradient of the objective function, ∇J, is defined by

$$\begin{aligned}\delta J(\varphi) &= \lim_{s\to 0} \frac{J(\varphi + s\,\delta\varphi) - J(\varphi)}{s} = \langle \nabla J, \delta\varphi \rangle \\ &= \left\langle \frac{\partial J}{\partial \varphi_L}, \delta\varphi \right\rangle + \left\langle \frac{\partial J}{\partial \varphi_U}, \delta\varphi \right\rangle,\end{aligned} \tag{3.6}$$

where $\delta\varphi$ is the first variation of the control. The functional δJ is the first variation of J with respect to $\delta\varphi$. The gradient may be expressed in terms of the solution of an *adjoint equation*. The complete derivation of the adjoint equations and the corresponding gradients are given in paper 5 in this thesis. Here we only state the final gradient expressions that rely on the adjoint state p and adjoint pressure denoted σ.

For the blowing and suction control the gradient becomes

$$\frac{\partial J}{\partial \varphi} = \int_{\Gamma_c} \psi \, \left(\varepsilon \varphi^T \, \psi - \sigma \right) \, \mathrm{d}\Gamma, \tag{3.7}$$

where ψ denotes the base functions for the control and Γ_c denotes the control interval.

For the initial condition control we can identify the gradient of the objective function (3.4) to be

$$\frac{\partial J}{\partial \varphi} = \frac{1}{c} \left[a\,\varphi - b\,p(0) \right],$$

where the constants a, b, and, c are defined as

$$a = \int_\Omega |u(T) - u_T(T)|^2 \, \mathrm{d}\Omega, \quad b = \int_\Omega |\varphi|^2 \, \mathrm{d}\Omega, \quad \text{and} \quad c = \left[\int_\Omega |\varphi|^2 \, \mathrm{d}\Omega \right]^2.$$

The first term of the gradient is due to the normalization of the objective function. Note that when we have reached optimum and the gradient is zero the initial condition is equal to the adjoint field times a scaling factor. Thus the optimality condition reads

$$\frac{\varphi}{E'(0)} = \frac{p(0)}{E'(T)}, \tag{3.8}$$

where E' denotes the disturbance energy.

Note that we discretize the expressions for the adjoint equations and the gradient that have been derived on the "continuous" level.

As mentioned the non-linearity in the state equation prohibits direct solution of the nonlinear optimization problem. Instead an iterative procedure is needed to find the optimal control. The general procedure is described in Figure 3.1. First, the governing equations (GE) are solved with an initial guess of φ. From the solution of the governing equations one can solve the corresponding adjoint equations (AE). Once the state and adjoint state are solved, we can construct the gradient of the objective function with respect to the control. We

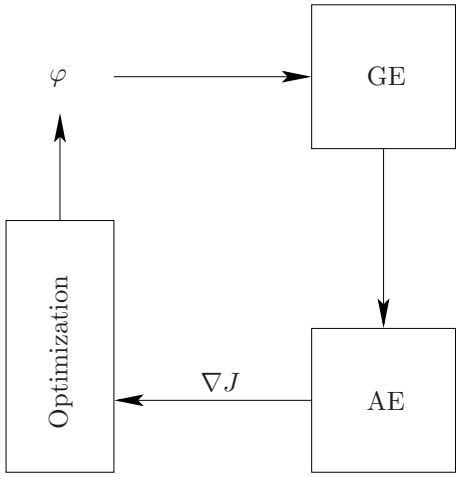

FIGURE 3.1. The optimization procedure. The control is denoted φ. The gradient of the objective function with respect to the control φ is denoted ∇J where J is the objective function. The governing equations and associated adjoint equations are denoted GE and AE respectively.

can then update the control with, for example, a conjugate gradient method or a quasi-Newton method. The whole loop is repeated until a satisfactory control is found.

The drawback with this kind of control is that it will only work under exactly the very conditions the control is constructed for. On the other hand, no a priori knowledge of the control is needed, and the performance obtained with the nonlinear optimization procedure often far exceeds the result from other simplified control finding approaches. One obvious application is to determine an upper limit of what is possible to achieve with a certain control scheme, something that might aid in the search for more efficient direct methods of control. Note however that this approach can be extended to a robust formulation that accounts for the worst case disturbances which makes the resulting control more general. This is described in Bewley *et al.* (2000). Another important issue for adjoint based control schemes is the choice of inner products. This choice could have impact a large impact on the convergence rate of the iterative process and also on how well the "optimal control" will work, see e.g. Protas & Bewley (2002).

3.3. Computational issues

The computational effort to solve the adjoint state is comparable to the solution of the state equation. Thus, the gradient can be determined by roughly the computational cost of solving two state equations, this cost being independent

of the number of degrees of freedom of the control parameterization. Note that the adjoint equations are always linear equations.

For unsteady simulations where the temporal history of the state equation is needed in the adjoint state computation the storage requirement can be very large. However, this requirement can be lowered using a *checkpointing technique*, see e.g. Berggren (1998). The price for the decreased storage demand is increased execution time. A memory reduction from N to $\sqrt{N}$, increases the computational cost with about a factor two.

Another important issue when deriving the discrete adjoint equations to be solved numerically is in what order the discretization takes place. One way is to discretize the expressions for the adjoint equations and the gradient that have been derived on the "continuous" level. An alternative is to discretize the Navier–Stokes equations and the objective function and *derive* the adjoint equations and the gradient expression on the discrete level. The latter approach leads to more accurate gradient directions, but is difficult to apply for the present discretizations. Issues related to the errors introduced by the approximative (continuous) formulation are discussed in e.g. Glowinski & He (1998) and Gunzburger (1998). The use of the continuous formulation is motivated by the findings in Högberg & Berggren (2000) where one conclusion is that it is sufficient to use the approximative (continuous) formulation in order to control strong instabilities. It was noted that in such cases, most of the reduction of the objective function is achieved in the first few iterations, and additional iterations only result in a fine tuning of the control. The drawback is that it will require more iterations to reach the true optimal solution, if it is even possible, than with the discrete formulation.

3.4. Results

3.4.1. *Blowing and suction control*

An example of nonlinear optimal control in action is shown in Figure 3.2 where cross-flow vortices in a Falkner–Skan–Cooke boundary layer are developing downstream. In the left plot the flow is uncontrolled whereas the nonlinear optimal control is active in the right plot. The results are taken from simulations in paper 5.

Two other examples are where two different Tollmien–Schlichting waves are introduced in Blasius boundary layer, one weak, and one stronger wave where nonlinear coupling effects start to appear. The weak TS-wave is generated by an oscillating two dimensional volume force with the dimensionless frequency $F = 200$, where $F = 2\pi f\nu/U_\infty^2 \times 10^6$. The volume force is centered at $x = 20$ and decays exponentially in both the x- and y-direction.

Domain and resolution data for the TS-wave simulations are given in paper 5. The Reynolds number at $x = 0$ in the computational box is 468.34 for both weak and strong disturbance. In the construction of the linear feedback kernels, the base flow profile is taken at $x = 150$. For the nonlinear optimization

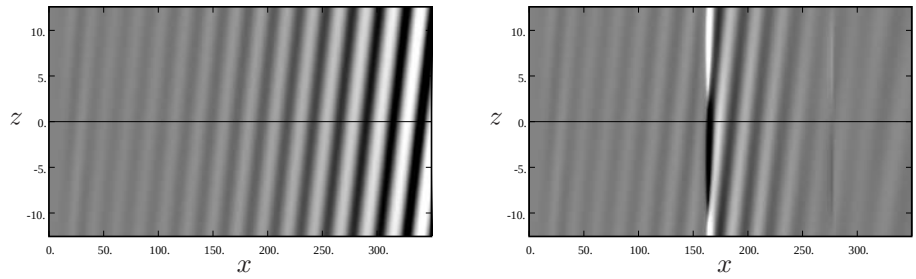

FIGURE 3.2. Snapshot of the wall normal velocity component in an x–z plane at $y = 0.5$ without control (left) and with nonlinear control (right). The control is applied in $x \in (145, 295)$. The black to white scale lies in the interval $v \in (-0.001, 0.001)$.

problem, we specify the observation interval in space and time to $x \in [75, 375]$ and $t \in [0, 750]$, respectively.

In Figure 3.3 the streamwise disturbance energy development of weak TS-waves are plotted. A small transient can be seen in the beginning of the energy curve, an effect that is due to the fact that we do not force a clean TS-wave. However, as the disturbance evolves downstream, a pure TS-wave emerges. The flow is perturbed just upstream of branch I of the neutral stability curve, which is at around $x \approx 27$, and the disturbance grows exponentially shown, as the solid line in Figure 3.3. The growth ends when branch II is reached at about $x \approx 219$. See for example Schmid & Henningson (2001) for details. The dashed line is the disturbance energy development with linear control active. Note that the exponential growth is switched to an exponential decay. With the nonlinear optimal control applied, the energy development follows the dash-dotted line. Since the energy levels are low and thus nonlinear effects negligible, we can conclude that the deviations originate from differences in the optimization problem and the limitations of the linear control. Analyzing the control signals shows no major differences between the two control approaches. The nonlinear control acts stronger in the beginning of the simulation and also stronger at the upstream part of the spatial control interval. These effects are a direct consequence of the limitations of the linear control problem formulation.

3.4.2. *Initial value control*

In this case the initial condition is constructed out of random modes to see whether the gradient procedure can find the optimal condition "far" from the optimum. For this particular case the gradient is reduced a factor 2000 and we reach a growth factor of in energy of 440.8 which is in good agreement with what linear stability theory predicts.

In figure 3.4 the starting initial condition and final optimal condition are shown. The optimal condition might still be improved somewhat though by,

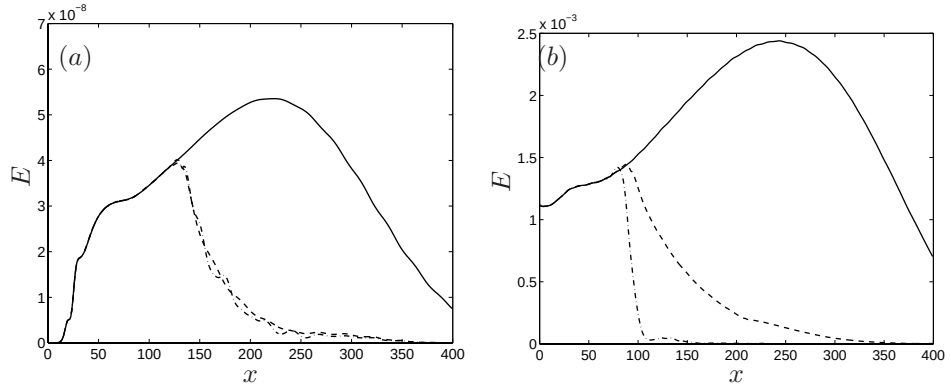

FIGURE 3.3. The spatial energy growth of a linear (a) and weakly nonlinear (b) TS-wave perturbation in a Blasius boundary layer without control from case 4 (solid), with linear control from case 5 (dashed), and nonlinear control from case 6 (dash-dotted). Control is applied in $x \in [75, 225]$. The TS-wave is generated at $R = 950$ for $\alpha = 0.30$. The linear controller is centered at $x = 150$.

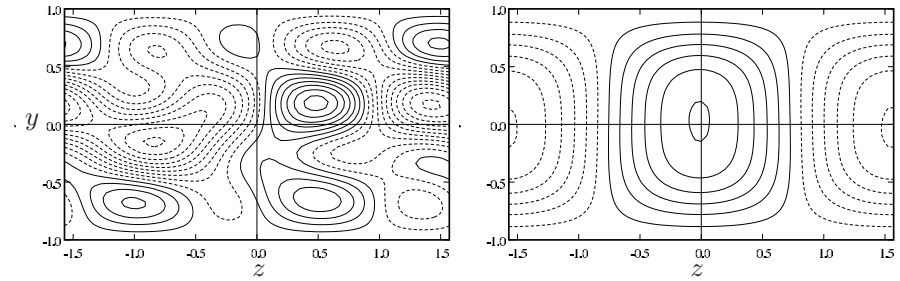

FIGURE 3.4. Contour plots of the wall-normal velocity component. The initial condition before (left) and after optimization (right).

for example, storing more forward velocity field. Note that these results are only a justification of the implementation.

CHAPTER 4

Direct numerical simulations

4.1. Pseudo-spectral collocation algorithm

All direct numerical simulations (DNS) of the three-dimensional, time-dependent, incompressible Navier–Stokes equations presented in paper 1, paper 3, paper 4, and paper 5 are performed with different versions of a pseudo-spectral algorithm which was first developed as a channel flow solver, described in Lundbladh *et al.* (1992). Based on the channel code a separate solver for boundary layer flows was developed which is reported in Lundbladh *et al.* (1999).

The time marching is performed with a four-step low-storage third-order Runge–Kutta method for advective terms and a Crank–Nicolson scheme for the viscous terms. A spectral method described in Canuto *et al.* (1988) is used with a Fourier discretization in streamwise and spanwise directions, and a Chebyshev collocation method in the wall-normal direction. The aliasing errors that are introduced when transforming the nonlinear terms back to Fourier space can be removed by increasing the physical space resolution by a factor 3/2 in the streamwise and spanwise directions. This can also be used for the Chebyshev polynomials. The discretization of, and the solution procedure for, the Navier–Stokes equations are described in Lundbladh *et al.* (1992). A similar algorithm was used by Kim *et al.* (1987).

Due to the fact that a spectral discretization has been used in the horizontal directions, which by definition means that we need a periodic flow in these directions, and the fact that we want to be able to simulate spatially evolving flows an additional non-physical forcing was added to the momentum equations in a downstream strip of the flow. The forcing blends the downstream base flow to the prescribed inflow condition and removes any disturbances in that the domain with a minimum of upstream influence. This is known as a *fringe region* technique and is described further in Lundbladh *et al.* (1999) and analyzed by Nordström *et al.* (1999). A similar technique was used by Bertolotti *et al.* (1992). The incompressible Navier–Stokes equations with the fringe forcing can be written as

$$\begin{aligned} \frac{\partial u}{\partial t} &= NS(u) + \lambda(x)(u - u_\lambda) + F, \\ \nabla \cdot u &= 0, \end{aligned} \tag{4.1}$$

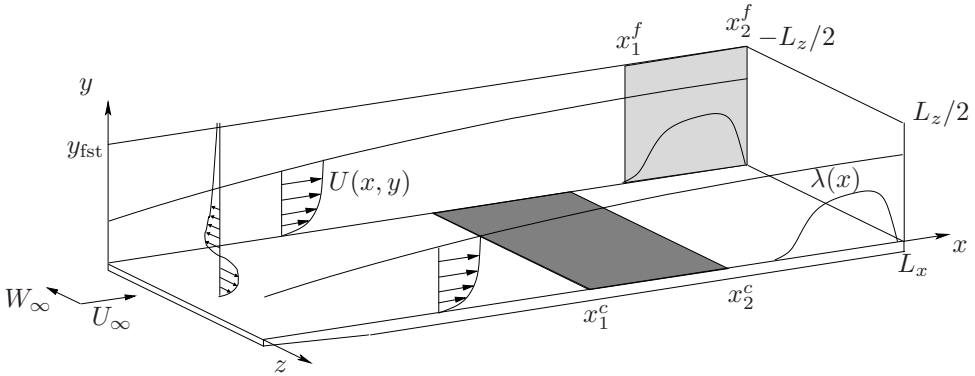

FIGURE 4.1. The computational box $[0, L_x] \times [0, y_{\text{fst}}] \times [-L_z/2, L_z/2]$ for the boundary layer flow case. The fringe forcing is applied in the region $[x_1^f, x_2^f]$. For all optimization problems the control region is $[x_1^c, x_2^c] \times [-L_z/2, L_z/2]$ which can also be limited only to a certain time interval $\times [T_1^c, T_2^c]$. The non-physical fringe forcing is applied in the domain $[x_1^f, x_2^f] \times [0, y_{\text{fst}}] \times [-L_z/2, L_z/2]$ where the amplitude is a smooth function $\lambda(x)$ with support in $[x_1^f, x_2^f]$.

where $\lambda(x)$ is a non-negative function and which is nonzero only at the end of the computational domain. The outflow and inflow conditions are determined by the desired velocity distribution u_λ. The additional forcing term $F = [F_1, F_2, F_3]$ is used for different things in spatial and temporal simulations. In temporal simulations it enforces a parallel mean flow whereas in the spatial simulations perturbations can be introduced with it.

The computational box is depicted in figure 4.1. For the solid walls no-slip boundary conditions are used. The freestream boundary condition in the boundary layer code, applied at $y = y_{\text{fst}}$ has to be sufficiently high in order not to influence the computational results. One choice used here is the Neumann boundary condition as an artificial freestream boundary. In order to decrease the box size in the wall-normal direction a generalization of the boundary condition used by Malik *et al.* (1985) can also be applied. It is an asymptotic condition that for each wavenumber pair exactly matches a potential flow solution decaying with the wall distance.

In the spatially evolving flows disturbances can be introduced into the flow by applying a volume forcing, either in the fringe region, or somewhere in the "physical" part of the flow domain, or by adjusting the boundary conditions in order to specify blowing and suction at the wall. In temporal flows disturbances are introduced through the initial condition. Different means of forcing are described in paper 4.

To solve the nonlinear optimization problem outlined in chapter 3, we need to compute the adjoint Navier–Stokes equations. The adjoint equations are solved in the same way as the Navier–Stokes equations, but with small modifications. However, the implementation of the optimization problem also requires the addition of a gradient based optimization routine as an outermost loop in the computations, which iteratively marches the Navier–Stokes equations forward in time and the adjoint Navier–Stokes equations backward in time, in order to compute gradient information which in turn is used to improve the control. For this purpose a limited memory quasi-Newton method is used. The algorithm, L-BFGS-B (Byrd *et al.* (1994)), is available on the Internet (the web-link is given in the reference list next to Byrd *et al.* (1994)) and was used without modifications. It is an algorithm well suited for large nonlinear optimization problems, with or without bounds on the control variables. The BFGS method successively computes secant approximations of the Hessian matrix as the iterations proceed. The algorithm has been shown to work well for many different types of optimization problems. Paper 5 deals with the adjoint related simulations.

To solve the state estimation problem, additions were made to the code so that two "independent" simulations could be run side-by-side. Wall measurements are extracted from both simulations and this information is then used together with the estimation feedback law, that has been outlined in chapter 2 and further described in paper 3 and paper 4, to compute the additional volume forcing term applied to the estimator to make that flow converge to the actual flow.

4.2. Pseudo-spectral finite difference algorithm

The DNS of turbulent channel flow reported in paper 2 were performed with the code of Bewley *et al.* (2001) which is also a pseudo-spectral code with 3/2 dealiasing in the streamwise and spanwise directions. In the wall-normal direction a second-order finite difference technique is applied which is energy-conserving. The time integration is performed with a hybrid second-order Crank–Nicolson and third order Runge–Kutta method developed by Aksevoll & Moin (1995). In this scheme, the wall-normal derivatives are treated implicitly to improve the stability properties of the code when using blowing and suction boundary conditions at the walls. The pressure is updated through a fractional step method which also ensures the incompressibility condition.

Additions to this code were made in order to investigate estimator performance as well as computing two-point correlation of the forcing vector f described in section 2.2.5.

All the turbulent channel flow simulations are performed for constant mass-flux flow at $Re_\tau = 100$ in a computational box of size $4\pi \times 2 \times 4\pi/3$ in $x \times y \times z$ respectively. The resolution is $42 \times 64 \times 42$ Fourier, finite difference, Fourier modes. The Reynolds number in the turbulent simulations is kept quite low at this stage for reasons of computational expediency.

CHAPTER 5

Conclusion and summary

The main work in this thesis has been devoted to studies of two different optimal control approaches where the objective has been to estimate and control transitional channel and boundary layer flows. Both approaches aim at finding the optimal blowing and suction control continuously distributed over the walls bounding the flow.

In the first approach we construct a linear optimization problem where the Orr–Sommerfeld/Squire equations are used to model the small perturbation dynamics and an objective function that measures the perturbation energy is chosen. By using tools from linear control theory it is possible to solve the optimization problem off line and construct a feedback control law based on solution of the optimization problem.

In the first study we use linear control theory to solve the optimization problem. Since the linear state-feedback control requires complete flow field information we combine it with a state estimator where noisy measurements of skin-friction and pressure are measured and used to reconstruct the state. The formulation of the state estimator is based on expected statistics of the initial conditions, the sensor noise, and the external disturbances acting on the system. The performance of the estimator is directly related to how well these statistical models describe flow. In the present work physically relevant models are suggested which give good performance of the estimator in transitional channel flows.

The importance of proper stochastic modeling of the sensor noise and the external disturbances is further stressed when a turbulent channel flow is estimated based on similar noisy wall measurements.

Based on the same idea with physically relevant parameterization of the stochastic models for the sensor noise and the external disturbances as for the estimator in channel flow it is demonstrated that the estimator also works in spatially developing boundary layer flows. Furthermore the estimator is combined with linear feedback control into a compensator where the controller is based on the reconstructed state in the estimator. The compensator control is shown to work well for different transition scenarios such as Tollmien–Schlichting waves, optimal perturbations, inflectional instabilities in the form of cross-flow vortices in Falkner–Skan–Cooke boundary layers.

In the second part of the study we formulate and solve a nonlinear optimization problem which means that we can use the full incompressible Navier–Stokes equations to model the flow. The objective function, which is the quantity we want to minimize, is defined to measure the perturbation energy. A standard method to solve this type of optimization problem is to iteratively solve the Navier–Stokes and adjoint Navier–Stokes equations to compute gradient information of the objective function with respect to the control parameterization which can then be used to update the control signal.

The strength of the nonlinear method is that we can take the complete flow physics into account and that we can optimize basically any property of the flow by constructing the proper objective function. The main drawback when applied to flow control is that it cannot be used online and that it is a computationally expensive method.

The nonlinear optimal control is compared with a linear optimal control computed for the same flow configuration and it is shown that the performance is similar for linear perturbations whereas when the disturbances get stronger the nonlinear optimal control is able to do better. However the main conclusion from this study is that the linear controller performs surprisingly well even when nonlinear interactions start to take place.

CHAPTER 6

Papers and authors contributions

Paper 1

State estimation of wall bounded flow systems. Part 1. Laminar flows
J. Hœpffner (JH), M. Chevalier (MC), T. R. Bewley (TB) & D. S. Henningson (DH). Submitted to *J. Fluid Mech.*

This paper considers the estimation problem, using a Kalman filter based on the linearized Navier–Stokes equations and appropriate stochastic models for the relevant statistics of the initial conditions, sensor noise, and external disturbances acting on the system. We show that a physically relevant parameterization of these statistics is key to obtaining well resolved feedback kernels with appropriate spatial extent for all three types of flow measurements available on the wall. The control theory aspects have been investigated by JH as well as implementation and testing of the plain Kalman filter. The estimator has been implemented and tested by MC in direct numerical simulations. The paper has mainly been written by JH in collaboration with MC, TB, and DH.

Paper 2

State estimation of wall bounded flow systems. Part 2. Turbulent flows
M. Chevalier (MC), J. Hœpffner (JH), T. R. Bewley (TB) & D. S. Henningson (DH). Submitted to *J. Fluid Mech.*

This work aims at estimating a turbulent channel flow at based on a time history of noisy wall measurements of the flow. We do this by applying a plain Kalman and an extended Kalman filter based on the linearized Navier–Stokes equations together with a stochastic model based on statistics gathered from a direct numerical simulations (DNS) of the same turbulent flow we aim to estimate. The implementation of the estimator and gathering of the statistics have been performed by MC. The implementation to solve the optimal estimation gains is done by JH. All direct numerical simulations are is done by MC. The writing has been done mainly by MC in collaboration with JH, TB, and DH.

Paper 3

Linear compensator control of a pointsource induced perturbation in a Falkner–Skan–Cooke boundary layer

M. Högberg (MH), M. Chevalier (MC) & D. S. Henningson (DH). *Phys. Fluids* 2003 **15**, 2449–2452

A pointsource induced perturbations on an infinite swept wing is controlled using linear control theory. Based on wall measurements in a spatial simulation of localized disturbances in a Falkner–Skan–Cooke boundary layer, an extended Kalman filter is used to estimate the full three-dimensional wave packet. The estimated field is in turn used to calculate a feedback control which changes the growth of the disturbance into decay. The implementation of the controller and estimator was done by MH. Simulations were performed by MH and MC. Writing was done mainly by MC in collaboration with MH and DH.

Paper 4

Linear feedback control and estimation applied to instabilities in spatially developing boundary layers

M. Chevalier (MC), J. Hœpffner (JH), E. Åkervik (EÅ) & D. S. Henningson (DH). To be submitted

This paper considers the estimation problem, using a Kalman filter based on the linearized Navier–Stokes equations and appropriate stochastic models for the relevant statistics of the sensor noise and external disturbances acting on the system. The compensator is applied and tested on a range of different types of transition scenarios. The estimator was implemented and verified by MC in a direct numerical solver. JH implemented the algorithm to compute the optimal estimation gain. The direct numerical simulations were performed by MC and EÅ. The writing of the paper was mainly done by MC in collaboration with JH, EÅ and DH.

Paper 5

Adjoint based control of channel and boundary layer flows

M. Chevalier (MC), M. Högberg (MH), M. Berggren (MB) & D. S. Henningson (DH). TRITA-MEK 2004:12

The implementation and verification of different adjoint based control strategies are reported. The performance of a linear and nonlinear optimal controller is compared for a few different flow cases. The adjoint channel flow solver to optimize blowing and suction control in the boundaries was implemented by MH. The corresponding adjoint solver for boundary flows was implemented by MC. The adjoint channel code that optimizes the initial condition to maximize the energy growth was implemented and tested by MC. The writing was mainly done by MC and MH in collaboration with DH and MB. The comparison between the linear and nonlinear optimal control has been published as an AIAA paper at the 3rd Theoretical Fluid Mechanics Meeting, St. Louis, MO (AIAA 2002-2755). The development and testing of the adjoint solvers is published as a technical report at the Swedish Defence Research Agency (FOI-R--0182--SE), 2001.

The papers are re-set to the present thesis format.

Acknowledgment

First of all I would like to thank my advisor Professor Dan Henningson for his guidance in the realm fluid dynamics and for generously sharing his knowledge but also for his complete and dedicated support when needed.

Many thanks also to Professor Thomas Bewley who arranged for an enjoyable four-month stay at UCSD and to his students Haoxiang, Laura, Patricia, and Bartosz.

I also want to thank Doctor Martin Berggren for his invaluable help in everything from mathematics to type setting of reports and Doctor Ardeshir Hanifi for always sharing his time and knowledge.

Thanks also to my colleagues at the Department of Computational Physics at FOI and the Department of Mechanics for providing nice environments to work in. In particular I would like to thank Jerome Hœpffner and Markus Högberg for all their help and assistance and dedicated work. I truly learned a lot from you both. Thanks also to Janne, Ori, Luca, Astrid, Espen, Martin, Arnim, and Erik for always giving me a warm welcome and for sharing your office space.

Finally I want to thank my family and my friends for supporting me throughout my studies.

The financial support from the Swedish Defence Research Agency (FFA/FOI) is greatfully acknowledged.

Tack Anna för allt ditt tålamod och stöd under alla omständigheter ♡

Tack Ida för dina mjuka kramar och glada tillrop efter långa dagar ♡

Bibliography

Abergel, F. & Temam, R. 1990 On some control problems in fluid mechanics. *Theoret. Comput. Fluid Dyn.* **1**, 303–325.

Aksevoll, K. & Moin, P. 1995 Large eddy simulations of turbulent confined coannular jets and turbulent flow over a backward facing step. Technical Report Report TF-63. Thermosciences Division, Dept. of Mech. Eng., Stanford University.

Anderson, B. & Moore, J. 1979 *Optimal filtering*. Prentice-Hall.

Andersson, P., Berggren, M. & Henningson, D. S. 1999 Optimal disturbances and bypass transition in boundary layers. *Phys. Fluids* **11**, 134–150.

Berggren, M. 1998 Numerical solution of a flow-control problem: vorticity reduction by dynamic boundary action. *SIAM J. Sci. Comp.* **19** (3), 829–860.

Bertolotti, F. P., Herbert, T. & Spalart, P. R. 1992 Linear and nonlinear stability of the Blasius boundary layer. *J. Fluid Mech.* **242**, 441–474.

Bewley, T. R. 2001 Flow control: New Challenges for a New Renaissance. *Prog. Aero. Sci.* **37**, 21–58.

Bewley, T. R. & Liu, S. 1998 Optimal and robust control and estimation of linear paths to transition. *J. Fluid Mech.* **365**, 305–349.

Bewley, T. R., Moin, P. & Temam, R. 2001 DNS-based predictive control of turbulence: an optimal benchmark for feedback algorithms. *J. Fluid Mech.* **447**, 179–225.

Bewley, T. R. & Protas, B. 2004 Skin friction and pressure: the "footprints" of turbulence. *Physica D* **196**, 28–44.

Bewley, T. R., Temam, R. & Ziane, M. 2000 A general framework for robust control in fluid mechanics. *Physica D* **138**, 360–392.

Byrd, R. H., Peihuang, L., Nocedal, J. & Zhu, C. 1994 A limited memory algorithm for bound constrained optimization. Technical Report NAM-08. EECS Department, Northwestern University, `http://www.netlib.org/toms/778`.

Canuto, C., Hussaini, M. Y., Quarteroni, A. & Zang, T. A. 1988 *Spectral Methods in Fluids Dynamics*. Springer.

Cathalifaud, P. & Bewley, T. R. 2004*a* A noncausal framework for model-based feedback control of spatially-developing perturbations in boundary-layer flow systems. part 1: Formulation. *Systems and Control Letters* **51** (1), 1–13.

Cathalifaud, P. & Bewley, T. R. 2004*b* A noncausal framework for model-based feedback control of spatially-developing perturbations in boundary-layer flow

systems. part 2: Numerical simulations using state feedback. *Systems and Control Letters* **51** (1), 15–22.

Collis, S., Chang, Y., Kellogg, S. & Prabhu, R. D. 2000 Large eddy simulation and turbulence control. AIAA Paper 2000–2564.

Gelb, A. 1974 *Applied Optimal Estimation*. MIT Press.

Glowinski, R. 1991 *Finite element methods for the numerical solution of incompressible viscous flow. Introduction to the control of the Navier–Stokes equations*, pp. 219–301. *Lectures in Appl. Math.* 28. American Mathematical Society, Providence, RI.

Glowinski, R. & He, J. 1998 On shape optimization and related issues. In *Computational Methods for Optimal Design and Control* (eds. J. Borggaard, J. Burns, E. Cliff & S. Schreck), pp. 151–179. Birkhäuser, Boston.

Gunzburger, M., Hou, L.-S. & Svobodny, T. P. 1989 Numerical approximation of optimal control problem associated with the Navier–Stokes equations. *Appl. Math. Lett.* **2**, 29–31.

Gunzburger, M., Hou, L.-S. & Svobodny, T. P. 1992 Boundary velocity control in incompressible flow with an application to viscous drag reduction. *SIAM J. Control Optim.* **30**, 167–181.

Gunzburger, M. D. 1998 Sensitivities in computational methods for optimal flow control. In *Computational Methods for Optimal Design and Control* (eds. J. Borggaard, J. Burns, E. Cliff & S. Schreck), pp. 197–236. Birkhäuser, Boston.

Hanifi, A., Schmid, P. J. & Henningson, D. S. 1996 Transient growth in compressible boundary layer flow. *Phys. Fluids* **8**, 826–836.

He, J.-W., Chevalier, M., Glowinski, R., Metcalfe, R., Nordlander, A. & Periaux, J. 2000 Drag reduction by active control for flow past cylinders. In *Computational mathematics driven by industrial problems (Martina Franca, 1999)*, pp. 287–363. Berlin: Springer.

Henningson, D. S., Lundbladh, A. & Johansson, A. V. 1993 A mechanism for bypass transition from localized disturbances in wall-bounded shear flow. *J. Fluid Mech.* **250**, 169–207.

Hinze, M. & Kunish, K. 2000 Three Control Methods for Time Dependent Fluid Flow. *Flow, Turbulence and Combustion* **65** (3/4), 273–298.

Ho, C.-M. & Tai, Y.-C. 1998 Micro-electro-mechanical-systems (mems) and fluid flows. *Annu. Rev. Fluid Mech.* **30**, 579–612.

Hu, H. & Bau, H. 1994 Feedback control to delay or advance linear loss of stability in planar poiseuille flow. In *Proc. R. Soc. Lond. A*, , vol. 447, pp. 299–312.

Huang, W. & Sloan, D. M. 1993 The pseudo-spectral method for solving differential eigenvalue problems. *J. Comp. Phys.* **111**, 399–409.

Högberg, M. 2001 Optimal Control of Boundary Layer Transition. PhD thesis, Royal Institute of Technology, Department of Mechanics, Stockholm, Sweden.

Högberg, M. & Berggren, M. 2000 Numerical Investigation of Different Discretization Approaches for Optimal Control. *Flow, Turbulence and Combustion* **65** (3/4), 299–320.

Högberg, M., Bewley, T. R. & Henningson, D. S. 2003*a* Linear feedback control and estimation of transition in plane channel flow. *J. Fluid Mech.* **481**, 149–175.

Högberg, M., Bewley, T. R. & Henningson, D. S. 2003*b* Relaminarization of

Re_τ=100 turbulence using gain scheduling and linear state-feedback control. *Phys. Fluids* **15**, 3572–3575.

Högberg, M. & Henningson, D. S. 2002 Linear optimal control applied to instabilities in spatially developing boundary layers. *J. Fluid Mech.* **470**, 151–179.

Joshi, S. S., Speyer, J. L. & Kim, J. 1995 Modeling and control of two dimensional poiseuille flow. *34th IEEE Conf on Decision and Control* pp. 921–927.

Joslin, R. D., Gunzburger, M. D., Nicolaides, R. A., Erlebacher, G. & Hussaini, M. Y. 1997 A Self-contained, Automated Methodology for Optimal Flow Control Validated for Transition Delay. *AIAA Journal* **35** (5), 816–824.

Jovanović, M. R. & Bamieh, B. 2001 Modelling flow statistics using the linearized Navier–Stokes equations. In *Proceedings of the 40th IEEE Conference on Decision and Control*, pp. 4944–4949. Orlando, FL.

Kailath, T. 1973 Some new algorithms for recursive estimation in constant linear systems. *IEEE transaction on information theory* **IT-19** (6), 750–760.

Kim, J. 2003 Control of turbulent boundary layers. *Phys. Fluids* **15** (5), 1093–1105.

Kim, J., Moin, P. & Moser, R. D. 1987 Turbulence statistics in fully developed channel flow. *J. Fluid Mech.* **177**, 133–166.

Lewis, F. L. 1986 *Optimal estimation*. New York: Wiley.

Lewis, F. L. & Syrmos, V. L. 1995 *Optimal control*. Wiley-Interscience.

Luchini, P. 2000 Reynolds-number-independent instability of the boundary layer over a flat surface: optimal perturbations. *J. Fluid Mech.* **404**, 289–309.

Lundbladh, A., Berlin, S., Skote, M., Hildings, C., Choi, J., Kim, J. & Henningson, D. S. 1999 An Efficient Spectral Method for Simulations of Incompressible Flow over a Flat Plate. Technical Report TRITA-MEK 1999:11. Department of Mechanics, Royal Institute of Technology, KTH.

Lundbladh, A., Henningson, D. S. & Johansson, A. 1992 An Efficient Spectral Integration Method for the Solution of the Navier–Stokes Equations. Technical Report FFA TN 1992-28. The Aeronautical Research Institute of Sweden, FFA.

Malik, M. R., Zang, T. A. & Hussaini, M. Y. 1985 A spectral collocation method for the Navier–Stokes equations. *J. Comp. Phys.* **61**, 64–88.

Nordström, J., Nordin, N. & Henningson, D. S. 1999 The fringe region technique and the Fourier method used in the direct numerical simulation of spatially evolving viscous flows. *SIAM J. Sci. Comp.* **20** (4), 1365–1393.

Protas, B. & Bewley, T. R. 2002 Regularization opportunities in the adjoint analysis of multiscale systems. In *Advances in Turbulence IX* (eds. I. P. Castro, P. E. Hancock & T. G. Thomas). Proceedings of the Ninth European Turbulence Conference.

Schmid, P. J. & Henningson, D. S. 2001 *Stability and transition in shear flows*, *Applied Mathematical Sciences*, vol. 142. Springer-Verlag.

Sritharan, S. 1991*a* Dynamic programming of Navier–Stokes equations. *System Control Lett.* **16**, 299–307.

Sritharan, S. 1991*b* An optimal control problem for exterior hydrodynamics. In *Distributed Parameter Control Systems: New Trends and Applications* (eds. G. Chen, E. Lee, W. Littman & L. Markus), pp. 385–417. Marcel Dekker, New York.

Weideman, J. A. C. & Reddy, S. C. 2000 A matlab Differentiation Matrix Suite. *ACM Transaction of Mathematical Software* **26** (4), 465–519.

Yoshino, T., Suzuki, Y. & Kasagi, N. 2003 Evaluation of GA-based feedback control system for drag reduction in wall turbulence. In *Proc. 3rd Int. Symp. on Turbulence and Shear Flow Phenomena*, pp. 179–184.